EFFECTS OF PROPAGATION PATHS ON SURFACE-WAVE MAGNITUDE ESTIMATES

DAVID N. VON SEGGERN
SEISMIC DATA LABORATORY

SEPTEMBER 14, 1971

Prepared for
AIR FORCE TECHNICAL APPLICATIONS CENTER
Washington, D.C.

Under
Project VELA UNIFORM

Sponsored by
ADVANCED RESEARCH PROJECTS AGENCY
Nuclear Monitoring Research Office
ARPA Order No. 1714

TELEDYNE GEOTECH
ALEXANDRIA LABORATORIES

APPROVED FOR PUBLIC RELEASE: DISTRIBUTION UNLIMITED.

DISCLAIMER NOTICE

THIS DOCUMENT IS THE BEST QUALITY AVAILABLE.

COPY FURNISHED CONTAINED A SIGNIFICANT NUMBER OF PAGES WHICH DO NOT REPRODUCE LEGIBLY.

Neither the Advanced Research Projects Agency nor the Air Force Technical Applications Center will be responsible for information contained herein which has been supplied by other organizations or contractors, and this document is subject to later revision as may be necessary. The views and conclusions presented are those of the authors and should not be interpreted as necessarily representing the official policies, either expressed or implied, of the Advanced Research Projects Agency, the Air Force Technical Applications Center, or the U S Government.

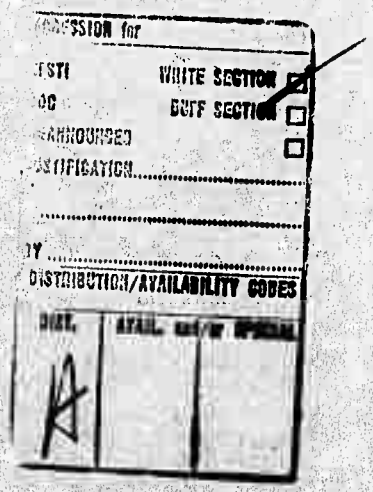

Unclassified
Security Classification

DOCUMENT CONTROL DATA - R&D
(Security classification of title, body of abstract and indexing annotation must be entered when the overall report is classified)

1. ORIGINATING ACTIVITY (Corporate author)
TELEDYNE GEOTECH
ALEXANDRIA, VIRGINIA

2a. REPORT SECURITY CLASSIFICATION
Unclassified

2b. GROUP

3. REPORT TITLE
EFFECTS OF PROPAGATION PATHS ON
SURFACE-WAVE MAGNITUDE ESTIMATES

4. DESCRIPTIVE NOTES (Type of report and inclusive dates)
Scientific

5. AUTHOR(S) (Last name, first name, initial)
von Seggern, D.H.

6. REPORT DATE
14 September 1971

7a. TOTAL NO. OF PAGES
~~80~~ 83

7b. NO. OF REFS
20

8a. CONTRACT OR GRANT NO.
F33657-72-C-0009

b. PROJECT NO.
VELA T/2706

c. ARPA Order No. 1714

d. ARPA Program Code No. 2F-10

9a. ORIGINATOR'S REPORT NUMBER(S)
279

9b. OTHER REPORT NO(S) (Any other numbers that may be assigned this report)

10. AVAILABILITY/LIMITATION NOTICES
APPROVED FOR PUBLIC RELEASE; DISTRIBUTION UNLIMITED.

11. SUPPLEMENTARY NOTES

12. SPONSORING MILITARY ACTIVITY
Advanced Research Projects Agency
Nuclear Monitoring Research Office
Washington, D.C.

13. ABSTRACT

In this report we investigate the effect of realistic propagation paths on the visual and spectral amplitudes of fundamental mode Rayleigh waves. We show that the Harkrider amplitude response factor of a layered media should relate directly to a station correction; it varies by a factor of nearly three between oceanic and continental sites. Attenuation due to effective Q losses may cause scatter, of over one-half magnitude unit, in teleseismic amplitudes but is unimportant at regional distances. Differences in recorded amplitude caused by dispersion over oceanic and continental paths are sufficient to warrant the application of path corrections to visually measured amplitudes. These differences can be avoided by computing spectra of the signals, or suppressed somewhat by using the results of stationary-phase approximations. More uniform propagation path effects at periods longer than 20 seconds suggests that use of 40 or 50 second waves would provide better seismic discrimination capability and better yield estimation.

14. KEY WORDS

Seismic surface-wave amplitude
Seismic surface-wave magnitude
Seismic attenuation
Stationary phase approximation
Airy phase
Earth layering response

Unclassified
Security Classification

EFFECTS ON PROPAGATION PATHS ON SURFACE-WAVE MAGNITUDE ESTIMATES

SEISMIC DATA LABORATORY REPORT NO. 279

AFTAC Project No.:	VELA T/2706
Project Title:	Seismic Data Laboratory
ARPA Order No.:	1714
ARPA Program Code No.:	2F-10
Name of Contractor:	TELEDYNE GEOTECH
Contract No.:	F33657-72-C-0009
Date of Contract:	01 July 1971
Amount of Contract:	$ 1,290,000
Contract Expiration Date:	30 June 1972
Project Manager:	Royal A. Hartenberger (703) 836-7647

P. O. Box 334, Alexandria, Virginia

APPROVED FOR PUBLIC RELEASE; DISTRIBUTION UNLIMITED.

TABLE OF CONTENTS

LIST OF TABLES

LIST OF FIGURES

ABSTRACT

In this report we investigate the effect of realistic propagation paths on the visual and spectral amplitudes of fundamental mode Rayleigh waves. We show that the Harkrider amplitude response factor of a layered media should relate directly to a station correction; it varies by a factor of nearly three between oceanic and continental sites. Attenuation due to effective Q losses may cause scatter, of over one-half magnitude unit, in teleseismic amplitudes but is unimportant at regional distances. Differences in recorded amplitude caused by dispersion over oceanic and continental paths are sufficient to warrant the application of path corrections to visually measured amplitudes. These differences can be avoided by computing spectra of the signals, or suppressed somewhat by using the results of stationary-phase approximations. More uniform propagation path effects at periods longer than 20 seconds suggests that use of 40 or 50 second waves would provide better seismic discrimination capability and better yield estimation.

INTRODUCTION

In the estimation of surface-wave magnitude, the raw data are Rayleigh wave signals at several stations. These time series must be condensed into single values; in addition to choosing a particular cycle of motion on the time record or a particular frequency point in the spectrum to give this value, certain corrections for the propagation paths are necessary. The choice of where to measure is not totally objective and systematic in seismological practice, and the corrections for the propagation paths are not fully defined. Observed Rayleigh waves at different azimuths but the same distance from an event can vary considerably in visual character and by large factors of amplitude at any particular frequency.

A recorded surface-wave signal can be represented schematically as the end result of the process:

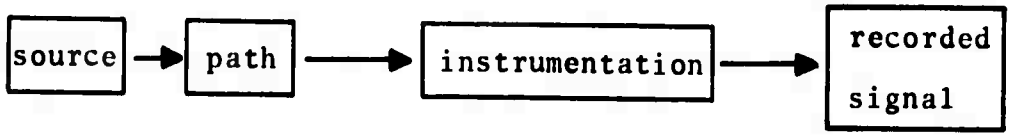

where each step involves a convolution in the time domain. Because of the more easily describable and predictable nature of long-period surface waves, as opposed to short-period body waves, we are able to investigate the effects of the source and the path on M_S determinations in a relatively complete manner. The

source effects are represented by radiation patterns of energy from equivalent force systems and have been discussed by von Seggern (1969), who showed how M_s of an earthquake is dependent upon depth of focus, azimuth from the source to the recording station(s), and the orientation of the double-couple forces. It was concluded that the distribution of stations and the source geometry could cause some earthquakes to appear like explosions when the M_s vs m_b discriminant was applied.

In this report we investigate the effects of travel path on estimates of M_s by examining amplitude response factors, attentuation losses, and dispersion characteristics of different earth structures. Specifically, we desire to know whether a factor dependent on propagation path can be removed from the observed amplitudes of Rayleigh waves so that the variance of M_s determinations at several stations for a single event can be reduced and so that a single M_s determination would be more closely related to yield or seismic moment. Since it has already been shown that the variance of m_b is almost twice that of M_s (von Seggern, 1970; Ericsson, 1971), we believe it is better to use surface waves (or long-period body waves) to estimate those parameters.

SEPARATION OF SURFACE WAVE SIGNALS INTO SOURCE, PATH AND RECEIVER FACTORS

Our representation follows that of Satô (1960) and is a straightforward convolution of all the time-domain elements which affect the surface wave signal, or alternatively a multiplication of frequency-domain elements. For Rayleigh waves propagating in a layered earth, the frequency-domain expression of a recorded signal is

$$W(\omega) = S(\omega)L(\omega)B(\omega)I(\omega) \qquad (1)$$

where

$S(\omega)$ = source spectrum

$L(\omega)$ = layer response

$B(\omega)$ = attenuation spectrum

$I(\omega)$ = instrument response

We consider each of these factors separately in the following sections. We will also examine dispersion, which is actually part of the layer response but which deserves to be considered separately because it strongly affects the shape of recorded waveforms.

Source spectrum

We consider as a source a simple point force, whose time variation has Fourier transform $F(\omega)$,

directed downward on the surface of the earth along the positive axis; the source spectrum is simply

$$S(\omega) = F(\omega)$$

To model more realistic sources we would use

$$S(\omega) = P(\omega)a^3 \tag{2a}$$

for explosions where P (ω) is the Fourier transform of the pressure time history at the equivalent cavity radius a and we might use

$$S(\omega) = F(\omega)d \tag{2b}$$

for earthquakes where F (ω) is the Fourier transform of the force time history of the simple components of the couple or double couple with moment arm(s) of length d. Note that both these realistic source functions have dimensions of force-length-time as opposed simply to force-time for a simple point force; therefore, for the layer response to them, a factor with units of length^{-1} must appear, multiplying the layer response to the single point force. This factor takes the form of the wavenumber k times some dimensionless expression for the radiation pattern.

Layer response

Layer response functions to various source models for realistic earth structures have been described by

Harkrider (1964) and Ben-Menahem and Harkrider (1964). The vertical component response to a single downward point force at or very near the surface of the earth is given by (Harkrider, equation (103)):

$$L(\omega) = A_R(\omega) H_0^{(2)}(kr) e^{-i\pi/2}$$

where A_R is the Rayleigh amplitude factor of Harkrider and $H_0^{(2)}$ is the zero'th-order Hankel function of the second kind. Beyond about a wavelength from the source, the expression can be well approximated by

$$H_0^{(2)}(kr) = (2/\pi kr)^{1/2} \exp[-i(kr-\pi/4)]$$

so that

$$L(\omega) = A_R(\omega) k^{-1/2} r^{-1/2} \exp[-i(kr+\pi/4)]$$

where the constants have been absorped in the amplitude factor $A_R(\omega)$. For the explosive source within 2 or 3 km of the surface, the layer response can be closely approximated by

$$L(\omega) = -\varepsilon_0(\omega) A_R(\omega) k^{1/2} r^{-1/2} \exp[-i(kr-3\pi/4)] \qquad (3a)$$

where ε_0 is the ellipticity of the Rayleigh wave at the surface, taken to be negative. Note the 180° phase difference between the response to a downward point force and the response to a spherical compressional source. Note also that the additional k factor preserves

the correct units. For the earthquake source, the corresponding medium response is

$$L(\omega) = A_R(\omega)k^{1/2}r^{-1/2}\exp[-i(kr-3\pi/4)]\chi(\omega) \qquad (3b)$$

where $\chi(\omega)$ is Ben-Menahem and Harkrider's radiation-pattern factor which was studied by von Seggern (1969) for its effects on magnitude estimates.

We are interested in the structure-dependent factors of the layer response to an explosive source in equation (3a): these are A_R, ε_o, and $k^{1/2}$. Outputs for numerous structures from HARKRIDER, a program which calculates Rayleigh-wave phase and group velocities as well as A_R, were available at the SDL. For these different structures which include oceanic, shield, and tectonic types we found that no value of ε_o or $k^{1/2}$ at a period of 20 seconds differed from another by more than 10%. These two factors can be considered to be constant for all structures, and a magnitude (M_s) correction for structure need not involve them. For periods longer than 20 seconds, ε_o and $k^{1/2}$ varied less among the structures, and for shorter periods they varied more. The factor A_R at 20 seconds, however, varied between 2.82×10^{-4} for a deep-ocean structure and 8.47×10^{-4} for a continental structure with a very thick crust. Harkrider and Anderson (1966) give the formal expression for A_R as

$$A_R = \left(2CU\int_0^\infty \rho(z)\left\{\left[\frac{\dot{u}^*(z)}{\dot{w}_0}\right]^2 + \left[\frac{\dot{w}(z)}{\dot{w}_0}\right]^2\right\}dz\right)^{-1}$$

where C and U are Rayleigh-wave phase and group velocity respectively, ρ is density, z is the depth, and the squared quantities are ratios of horizontal and vertical particle velocities at depth z to vertical particle velocity at the surface. The integral portion, as well as C and U, vary with structure and mode. Using all the available HARKRIDR outputs at the SDL, we show fundamental-mode A_R (at 20 seconds period) versus CU (at 20 seconds period also) in Figure 1. The predicted inverse dependence is evident, with upper points representing thick-crust continental structures and the lower two points representing deep-ocean structures. A simple straight line (visually adjusted) seems to fit the data adequately, since no point deviates from it by more than 10% on the vertical scale. Plots of A_R versus U in Figure 2 and A_R versus C in Figure 3 show reasonable straight-line approximation also, with scatter somewhat greater than for A_R versus CU. Thus, knowing either group or phase velocity of the medium, or preferably both, one could estimate the factor A_R directly within about 10%. Otherwise, one must invert the velocity data to obtain a structure and then compute A_R for the structure.

A further consideration in applying A_R corrections is that the propagation path is rarely a laterally homogeneous structure. For instance, what A_R is to be applied to a signal recorded on a continent, having originated in another continent, but having traversed an oceanic path for most of the epicentral distance? In the past Rayleigh wave propagation through gradual

changes in structure at the continental boundaries have been studied with models and approximated by wedges or even vertical discontinuities in theoretical solutions. Actual observations such as that by McGarr (1969) show a signal being amplified by a factor of 2 or 3 in crossing from oceanic to continental structure and deamplified by the same factor for the opposite direction. We point out that the A_R for oceanic structures is half as great as the average for continental structures (Figure 1), and this factor alone may be a simple means of predicting amplitude changes from one structure to another. Moreover, if the value of A_R at a point on a gradually changing structure controls the amplitude at that point, it may be necessary to know only A_R at the receiving station in order to apply the A_R correction to magnitude. Only the eventual solution of the Rayleigh-wave propagation problem in changing crust-mantle structures by finite-element schemes can provide the correct answers.

We regard the factor A_R as primarily a station correction. If, however, the structure in the source area immediately grades into quite dissimilar types, such as at a continental boundary, partition of the source energy into the various modes may vary significantly with azimuth. Considering now a source area homogeneous to a radius of at least a wavelength, such partition of energy would be the same at all azimuths; and observed amplitudes of signals which are recorded on different structures could be equalized by dividing them by this amplitude factor A_R appropriate to the

recording site. Using the extreme continental values of A_R, from approximately 4×10^{-4} to 8×10^{-4}, the largest correction to M_s would then amount to the logarithm of their ratio, 0.3, when no oceanic sites were involved. However, in practice, these extreme structures are seldom found, and we expect typical M_s corrections based on A_R to be much less than 0.3 when no oceanic sites are involved.

Attentuation

Brune (1962) showed that the attenuation factor for surface waves is given by

$$B(\omega) = \exp[-\omega r/2Q(\omega)U(\omega)] \qquad (4)$$

where Q is the dimensionless quality factor and U is the group velocity. Here Q is understood to be the "effective" Q over the path in question. Thus, measured Q for Rayleigh waves of 20 second period includes losses due to causes other than actual absorption; e.g., mode conversion and the various "optical" processes (reflection, refraction, diffraction, scattering).

Measured Q values for 20 second Rayleigh waves are not numerous; Tsai and Aki (1969) found that Q averaged approximately 700 for many paths from the Parkfield earthquake of 1966, Tryggvason (1965) found Q to be over 1000 for Asian and European paths, Marshal and Carpenter (1966) found it to be about 400 for the Novaya Zemlya to North America path. In these studies, the waves often traversed major structural boundaries. von Seggern (1970) found an average Q of

134 in the period range of 10 to 16 seconds for paths from NTS explosions to stations around the Western United States; this low value probably reflects the tectonic nature of the earth's crust and upper mantle there. From Figure 7 one can estimate the approximate value of Q required by the magnitude correction of Gutenberg (1945). If we compare the diminution predicted by spherical spreading and normal dispersion with the diminution predicted by -1.66 logΔ we see that the loss of amplitude required in addition to spreading and dispersion can be accounted for with Q of about 300 at T = 20 seconds, depending on the group velocity used in (4). Thus, Gutenberg's data gave a Q less than that of other investigators mentioned above.

Figure 4 shows the amplitudes to be expected for a plane wave propagating in a flat medium at distances from 0 to 10,000 km for Q values of 100, 200, 400 and 1000. From the evidence above, we believe that 100 and 1000 are the extreme possible limits to Q at 20 second periods over all possible earth paths. It appears that knowledge of Q is extremely important if observed amplitudes are to be corrected for propagation path. For stations 10,000 km from the source, amplitudes could vary by a factor of approximately 100 for the extreme limits of Q. Again, this result must be altered by the realization that two paths from a source in the earth could not be so extremely different in Q properties over thier entire length; and we should probably accept factors of 10 or less as being more realistic for the largest variation in amplitude due

to attenuation over two 10,000 km paths in the earth. For instance, 3.5 would be the ratio of amplitudes at 10,000 km over a structure with Q = 400 and another with Q = 200 (Figure 4). Note that for distances of 1000 km or less, amplitudes should vary by less than a factor of two even for the extreme Q differences.

Dispersion

The shape of the group-velocity curve affects the character of the recorded Rayleigh wave and therefore measured amplitudes. This is most dramatic in comparing seismograms over oceanic and continental paths. We can study the effect carefully if we construct synthetic seismograms over various earth structures and observe the amplitudes. We have already set down the various factors which comprise the Fourier transform of a Rayleigh wave from an explosion at or near the surface of the earth -- equations (2a), (3a), and (4). Combining these we have from (1):

$$W(\omega) = -a^3 P(\omega) \varepsilon_0(\omega) A_R(\omega) k^{1/2} r^{-1/2} \exp[-i(kr-3\pi/4)] \cdot \exp[-\omega r/2Q(\omega)U(\omega)] I(\omega)$$

Replacing k by ω/C, changing from cylindrical spreading to spherical spreading of the earth (using R_0 as the earth's radius), and defining the instrument response as

$$I(\omega) = G(\omega)e^{-i\phi(\omega)}$$

where G (ω) is the amplitude gain and φ(ω) is the phase lag, the transform of the recorded signal is

$$N(\omega) = \frac{-a^3 P(\omega) c_0(\omega) A_R(\omega) \omega^{1/2} \exp(-i[\omega r/C(\omega) + \phi(\omega) - 3\pi/4]) G(\omega)}{C(\omega)^{1/2} R_0^{1/2} \sin^{1/2}(r/R_0) \exp[\omega r/2Q(\omega)U(\omega)]}$$

Since up is positive on a seismogram and we have adopted the layering response of a medium with the z axis positive downward, we shift the phase an additional π or, equivalently, we change the sign of the whole expression; and to start the synthetic seismogram at some time later than the origin time, we subtract τ seconds from r/C, where τ is near the expected time of arrival of the wave group with the highest velocity:

$$N(\omega) = \frac{a^3 P(\omega) c_0(\omega) A_R(\omega) \omega^{1/2} G(\omega) \exp(-i\{\omega[r/C(\omega) - \tau] + \phi(\omega) - 3\pi/4\})}{C(\omega)^{1/2} R_0^{1/2} \sin^{1/2}(r/R_0) \exp[\omega r/2Q(\omega)U(\omega)]} \tag{5}$$

The recorded Rayleigh wave is then the inverse transform of (5):

$$w(t) = \int \frac{a^3 P(\omega) c_0(\omega) A_R(\omega) \omega^{1/2} G(\omega) \exp(i\{\omega[t + \tau - r/C(\omega)] - \phi(\omega) - 3\pi/4\})}{C(\omega)^{1/2} R_0^{1/2} \sin^{1/2}(r/R_0) \exp[\omega r/2Q(\omega)U(\omega)]} d\omega \tag{6}$$

A program was written (LPSYN) which takes as input all the frequency-dependent parameters needed in (5) at specified frequencies, interpolates them with straight lines, and uses a fast Fourier transform algorithm (COOL) to construct the signals represented by (6). $P(\omega)$ was taken to be the spectrum of a step function, $1/\omega$. From Brune (1969) the phase velocities for Shield, Mid-Continent, Basin and Range, Alpine, Great Island Arc, and Deep Ocean were used in synthesizing signals as given in Table I. The velocities were extrapolated to five second periods in all but the shield case. Since we are now just interested in the possible effects of dispersion on recorded amplitudes or magnitude determinations, we take the layer response ($\epsilon_o A_R k^{1/2}$) and attenuation (Q) to be identical for all these structures (knowledge of these would allow the amplitude measurement to be corrected for them in practice). The standard LRSM long-period response(Table IV) was used in the synthesis. Values of $Q(\omega)$ were taken from Isai and Abi (1969) and are given in Table II here along with the layer response used, which happens to be for a Gutenberg continental structure. For each new distance, t was set to begin the signals prior to the arrival time of the groups of maximum velocity. Figure 5a, then, shows the seismograms for each structure (except the oceanic) at epicentral distances from 100 km to 10,000 km. They are distinct for the five structures used. Unexpected high-frequency waves superimposed on the low-frequency first-arriving groups are an artifact of the synthesis technique and should be disregarded. Figure 5b shows the oceanic

signals, which are quite different from the continental examples at a given distance. Figure 5c shows seismograms for the mid-continent structure as in Figure 5a, except the Q values of Table II at 10 and 15 seconds were doubled; this was an attempt to simulate more closely NTS seismograms, dominant periods of which are characteristically 15 seconds or less even out to teleseismic distances.

It is evident that the most precise way of removing effects of dispersion is to Fourier transform the signal to get (5) so that dispersion effects are contained solely in the phase term and do not alter the amplitudes. If one does not have the time or machine capability for this step, the stationary phase approximation to (6) will indicate the effect of dispersion over various paths on amplitude visually measured at a certain period. This approximation (Kanth, 1968) can be given as a function of distance r and period T:

$$v(T,r) = \frac{a^3 P(T) c_0(T) A_R(T) U(T)}{r^{1/2} R_0^{1/2} \sin^{1/2}(r/R_0) C(T)^{1/2} I^{3/2} (dU/dT)^{1/2}} \qquad (7)$$

(The appendix shows the derivation of this.) The factor $R_0^{-1/2} \sin^{-1/2}(r/R_0)$ is in common with the expression for amplitude of a spectral component propagating over the earth; the new factor $r^{-1/2}$ applies to all periods, but the other factors, except for a^3, are dependent on period.

Relative amplitudes at a certain period for the six different structrues in Figures 5a and 5b should be given approximately, for any distance, by:

$$w(T_0) \propto U(T_0)\left(\frac{dU}{dT}\right)^{-1/2}_{T_0} \tag{8}$$

where we have neglected the very small variation (≤10%) of $C^{1/2}(T)$ in (7) (remember that the source spectra, layer response, and attenuation were made identical for these six structrues since we are not investigating their effects here). To check this, group velocity disperson curves were first determined from the synthetic seismograms at 10,000 km. These curves, shown in Figure 6, are somewhat sinuous due to the straight-line interpolation of the input phase velocities by the synthesis program. However, U and dU/dT can be fairly well determined at a period of 20 seconds, and these values for the six structures are given in Table III. Also in Table III are the peak-to-peak amplitudes measured for the six structures at 10,000 km for a period of 20 seconds, the exact position of the 20 second period being determined by the arrival time versus peak number data. These amplitudes show a factor of four between extremes. Dividing the measured amplitudes by the structure-dependent factors given by (8) should result in equalized amplitudes; however, the actual results, given in Table III also, show a factor of approximately 1.7 between the extremes of the equalized amplitudes.

Thus some equalization has been accomplished, but this could only be done after group velocity curves had been established and the arrival time of the wave group of 20 second period had been determined. If we disregard the oceanic structure, the equalization achieved using continental group-velocity data is negligible, since the measured raw amplitudes on the continental structures varied by only a factor of 2.2 at the most. The experiment was repeated at a period of 30 seconds for the continental structures, and the results (not listed) showed no benefit in applying (8) as a means of equalizing measured amplitudes. We conclude then that amplitude equalization for dispersion effects is beneficial only if oceanic paths are involved.

If we take from (7) the distance-dependent terms of $\sin^{-1/2}(r/R_0)$ for spherical spreading and $r^{-1/2}$ for the stationary phase approximation, the amplitude-distance relation for a given period T_0 using these is shown in figure 7. In the case when amplitude is measured at an Airy phase (group velocity minimum or maximum) the stationary-phase approximation is invalid and $r^{-1/2}$ is replaced by $r^{-1/3}$ (Kaith, 1968); the effect of this plus spreading on the Airy phase amplitude is also shown in figure 7, and it is clear that at teleseismic distances use of the Airy phase will give 0.2 - 0.3 higher values of M_s than amplitudes measured at periods where the group velocity curve is not flat. When the absorption term of (7) is added to the spreading and stationary-phase effects, the result is further diminution as shown in figure 7 also. A Q of 375 at T = 16

seconds was used in computing the absorption effect; this is approximately the same value as used in synthesizing the seismograms of Figure 5. Also U was taken equal to π although in fact it varies from 2.73 to 3.08 km/sec for the five continental structures. The line in Figure 7 which represents all the distance-dependent factors of (7) should then be the proper distance-correction factor for use on the synthetic seismograms of this report, or on any real siesmograms. We see that log A is not a linear function of log Δ over the entire range of 1° - 100°. But for the distance range Δ>15°, Gutenberg's (1945) correction factor of -1.66logΔ fits the theoretical diminution quite well as shown in Figure 7, where the intercept has been arbitrarily set for the Gutenberg correction. For Δ<15° von Seggern (1970) has suggested -1.09logΔ as a better fit to data in the western United States, and this slope conforms well to the theoretical diminution at Δ<15° with Q = 375 in Figure 7. There is a 0.33 magnitude unit hiatus at Δ = 15° between the Gutenberg line and the von Seggern line; the reason for this is given by von Seggern (1970). The same theoretical curve, only with Q = 134, which is the value actually determined in the Western United States by von Seggern, would still agree well with the -1.09logΔ correction out to 15° because the attenuation factor is small in either case (Figure 4). Thus, the stationary phase approximation giving $r^{-1/2}$ amplitude decrease may be valid to quite close distance even though the signal is not yet dispersed. (Figure 5 for 1000 km.) Good agreement in

slopes between theoretical diminution and empirical results for $1° < \Delta < 100°$ has been found. Obviously, the application of (8) to find the relative amplitudes at different periods on one seismogram fails at close distances where the wave groups of differing periods have not sorted themselves out.

Measuring maximum amplitudes from synthetic seismograms should enable us to relate variations in M_S to the known composition of these seismograms. The author calculated equivalent ground motion of the maximum peak-to-peak amplitude on the seismograms of Figure 5 by dividing the amplitude by the instrument response (Table IV) for the period of the maximum excursion. The amplitudes, corrected for instrument response and periods are given in Table V. The logarithms of the amplitudes are plotted in Figure 8 versus the logarithm of Δ, the epicentral distance in degrees. The teleseismic decay of amplitude predicted by Gutenberg and the regional decay by von Seggern are also plotted, along with the theoretical decay from Figure 7 when spreading ($\sin^{-1/2}[r/R_o]$), absorption ($\exp[-\omega r/2Q(\omega)U(\omega)]$) and the distance dependence of the stationary phase approximation ($r^{-1/2}$) are taken into account. Gutenberg's linear relation fits the synthetic data as well as or better than the arcuate relation predicted from theory at over 1600 km distance. In the stationary-phase approximation no account was taken of the changing period of the maximum excursion which is evident in the measured periods of Table V. Proper use of the stationary-phase approximation requires that we evaluate

the frequency-dependent factors in equation (7) as well as $r^{-1/2}$ for a given set of measurements at various distances when the dominant period is changing. We must consider the nearly three-fold increase of the medium response $\varepsilon_o A_R k^{1/2}$ (Table II) from 20 to 10 seconds, the two-fold decrease of the source amplitude spectrum P (ω), which we assumed to be $1/\omega$, from 20 to 10 seconds, and three-fold increase of $T_o^{-3/2}$ from 20 to 10 seconds. We cannot evaluate $U/(dU/dT)^{1/2}$ accurately at 10 seconds for the structures, but its effect must be to offset the result of the variation in the other factors because the measured amplitudes on the synthetic continental seismograms are in excellent agreement with the predicted arcuate relation over the entire distance range, even though this relation strictly applies to a constant dominant period.

The variation in the factors mentioned above explains the low oceanic amplitudes in Figure 8 because the dominant period of the oceanic seismograms is 5 to 10 seconds longer than that of continental ones. The amplitude diminution for the oceanic structure nearly follows a $-\log\Delta$ relation and differs considerably from Gutenberg's $-1.66\log\Delta$ relation.

Two other important lines are included in Figure 8. One is the $-1.09\ \log\Delta$ relation of von Seggern (1970) in its correct position relative to Gutenberg's curve. (As in Figure 7, this results in a 0.33 hiatus at $\Delta = 15°$ in the distance correction factor.) Evidently, the amplitudes from synthetic seismograms of this report do not agree with those from NTS seismograms.

The solid line merely confirms this conclusion, because it is a least-square fit to the NTS data out to $\Delta = 40°$ (von Seggern, 1971) and is a $-.90\log\Delta$ relation (with arbitrary intercept here). The seismograms of Figure 5c were synthesized with higher Q's at 10 to 15 second periods in an attempt to more closely approximate the NTS data on both sides of the 15° division. Results of measuring amplitude on these are shown by triangles in Figure 8. It is evident that Q's may need to be increased further and that the Airy phase may need to be more distinct before agreement is attained with the nearly $-\log\Delta$ relation of NTS amplitudes. Also, changing the source time function from the step used here to a decaying pulse should improve the agreement.

The problem of the dominant period taking large jumps, as for the shield structure between 200 and 400 km (Table V and Figure 8), which causes aberrations from a smooth amplitude-distance relation, and the vagaries of the period measurement combine to make the traditional M_s calculation an arbitrary and capricious datum for NTS Rayleigh waves, especially since the LRSM instrument response slopes at essentially 12 db/oct below a 20 seconds period. A magnitude estimate based on the spectrum of the signal should be more reliable. Using spectra and keeping the period invariant would require an amplitude-distance relation different from any of the three presented in Figure 8; its form would be (from equation (5)):

$$W(\omega) \propto R_o^{-1/2} \sin^{-1/2}(r/R_o) \exp[-\omega r/2Q(\omega)U(\omega)] \qquad (9)$$

MILROW AND BOXCAR AT COMMON STATIONS

Recently Evernden and Filson (1971) have suggested that the difference in the M_s-vs-yield behavior for Amchitka Island and NTS can be attributed solely to the fact that measurement of the surface wave amplitudes is made at much shorter periods for NTS events. They state that at a given yield amplitude spectra are equal at 20 second periods for the two sites, but they do not show individual spectra or indicate which stations were used to form this conclusion. We will show here spectral computations which contradict this supposed equivalence at 20 second periods.

We have chosen to compare the spectra of MILROW (Amchitka) and BOXCAR (NTS) at five teleseismic stations common to both events: NP-NT, WH2YK, PG2BC, RK-ON, and HN-ME. By using common stations, we should be minimizing effects of the medium response factor, $\epsilon_o A_R k^{1/2}$. By computing spectra, we should be eliminating any dispersion conditions which might affect visual amplitudes. Two of the above stations, NP-NT and WH2YK, were nearly equidistant from MILROW and BOXCAR and are particularly important in the comparison.

The spectra were computed from the unfiltered seismograms, digitized at 1 sample per second, using a fast Fourier transform subroutine. Lengths of 128, 256, or 512 points (seconds) were used. Since the time windows selected for spectral computation were never exactly one of these even powers of two, zeros were added to the signals and the computed amplitude spectra were

multipled by the factor

$$\left(\frac{N_s + N_z}{N_s}\right)^{1/2}$$

where

N_s = number of points in chosen time window of signal

N_z = number of zeros added to make even power of two

to make them valid estimates within the actual signal window chosen. The calibrations for the seismograms were carefully checked, and the spectral outputs were scaled in millimicrons. The instrument response has not been removed, and the spectra represent true ground motion at a period of 25 seconds only. One seismogram has an uncertain calibration -- MILROW at WWZVK. This was due to the fact that the sine-wave calibrator was inoperative for some time before the MILROW event and until the station closed. Magnification for this seimsogram had to be figured from a calibration obtained about two weeks prior to the event.

The spectra of the two events at the five common stations are shown in Figure 9, along with plots of the actual signals. Signal length in each case was controlled by the group velocities shown at the start and end of the signal plots.

The spectra must be equalized for yield and distance differences, and we will do this at the 20 second periods only. The yields for BOXCAR and MILROW are 1.2 and 1.0 Mt, respectively. Since amplitude at long periods is proportional to yield (von Seggern and Lambert, 1969), we multiply the BOXCAR amplitudes by the ratio of 1.0 over 1.2. To equalize the BOXCAR amplitudes to the MILROW distance, we use equation (9) with Q = 300 and U = τ. Recall that we determined that this value of Q satisfied Gutenberg's data. The group velocity is arbitrarily set equal to π km/sec. Equation (9) applied to the BOXCAR amplitudes means that we multiply by the factor

$$\left[\frac{\sin (r_B/R_o)}{\sin (r_M/R_o)} \right]^{1/2} \exp[-(r_B - r_M)/6000]$$

where subscripts B and M refer to BOXCAR and MILROW, respectively. The results of applying these yield and distance corrections are shown in Figure 9 also. At NP-NT and WH2YK the change is small, and the difference in amplitudes at 20 seconds between BOXCAR and MILROW is evident. There is approximately a factor of two at NP-NT and a factor of six at WH2YK. Because of the calibration difficulty stated above, the factor for WH2YK may be erroneous. Since the factor of six should be attributed to differences in Q over the two paths to WH2YK, a check with Figure 4 at 3000 km distance shows that only unrealistically disparate Q values

could satisfy this amplitude data. The factor of two at NP-NT, however, could be explained by reasonable Q values of 200 for the MILROW path and 700 for the BOXCAR path. Comparison of 20-second amplitudes at the other stations, PG2BC, RK-ON, and HN-ME, is not as simple because of the distance differences to the two sites. Again, though, the BOXCAR paths to these stations must have significantly higher Q's to satisfy the data.

Using common teleseismic stations, we find that the M_s (based on the spectral amplitude at 20 seconds period) of MILROW is distinctly lower than that of BOXCAR and therefore that the M_s vs yield relation for NTS events cannot be duplicated by Amchitka events, due to these attenuation differences.

CONCLUSIONS

Hopefully, we have illuminated the more important quantities which cause variation in Rayleigh wave amplitudes from site to site. These quantitites are the medium amplitude response A_R, the attenuation due to effective Q, and the stationary-phase approximation for dispersed waves. All three deserve consideration when visual amplitudes are used to calculate M_s, but only the first two when spectra are used. Another factor which may be important is multipathing, but it was not considered here because it cannot be studied in a general sense. Capon (1970) shows the multiple paths inferred from analysis of LASA recordings of distant events along with real and synthetic seismograms exhibiting multiple-path effects, and this facet of propagation may be significant in relation to magnitude estimation.

It was found that the medium response factor A_R could vary by at most approximately a factor of three (0.5 on M_s scale) between continental structrues and oceanic structrues. Exactly how well the amplitude at a given site can be related to this factor depends on how rapidly the structure is changing in the vicinity of the site. It is possible that oceanic island stations would record amplitudes almost identical to ocean-bottom stations nearby on ideal oceanic structure because the horizontal dimension of the transition to the island structure is less than a wave-length or two of the periods of interest. We believe that as much as 0.3 of the large negative magnitude differences from

the average event magnitude of island stations AD-IS (SDL shot report, BRONZE) and HW-IS (SDL shot report, BILBY) can be explained by the medium response factor, since these were the only oceanic sites for the two events.

The effect of Q differences can be very significant, increasing with teleseismic distance. For this reason, when Q is unknown for periods of 10 to 50 seconds, surface wave data from regional-distance stations would be weighted more in discrimination work and for estimating yields and seismic moments. This conclusion was substantiated by comparing MILROW and BOXCAR spectra at common stations.

Dispersion of the Rayleigh wave has a pronounced effect on amplitude between oceanic and continental structures -- a factor of three or more. It was previously stated that AD-IS and HW-IS had anomalously low magnitudes for NTS events; they were actually about 0.8 magnitude units lower than the event averages. We attributed about 0.3 of this to the medium response factor above; and here we attribute the remaining 0.5 to dispersion effects such as illustrated in Figure 8 for the synthetic oceanic seismograms at the distances in question, about 40°. The lower (approximately 0.4) surface wave magnitudes of LONG SHOT across western North America relative to more easterly parts (Lambert et al., 1969) might be in part attributed to the fact that paths to the Western stations comprised mostly oceanic structure. If only continental paths are under consideration, the

dispersion effect is not significant, as shown by the clustering of magnitude values in Figure 8 for teleseismic distances at least. Dispersion corrections based on the stationary-phase approximation for continental paths probably does not warrant the effort, especially since this approximation is difficult to evaluate in practice.

The use of spectra to estimate M_s would obviate the requirement for a dispersion correction for every path and would also allow one to escape pitfalls such as sudden jumps in the predominant period with distance. These jumps can cause magnitudes at regional distances to vary erratically if one adheres to the rule of measuring the maximum amplitude on the seismogram. This pitfall is somewhat analogous to the problem with body-wave magnitude when different branches of the travel time curve lie close together. Also for this reason, visual surface wave data at regional distances should be weighted less than that at teleseismic distances; this balances the ill effects of Q on teleseismic surface-wave amplitudes. If spectra are used, however, the regional data should still be more reliable.

Finally, we wish to emphasize the advantages of using longer periods, say 50 seconds, in determining M_s. We already know that due to differences in source parameters (depth, dimensions, time function) the M_s vs m_b criterion seems to discriminate even better at longer periods than at 20 seconds (Molnar et al., 1969). In addition, all the propagation factors which affect M_s values as discussed in this report are much less

variable among typical earth structures at periods of 50 seconds than at periods of 20 seconds. The amplitude response of a layered medium, A_R, differs by only a factor of at most 1.5 at 50 seconds periods for the same group of structures for which Figure 1 showed a factor of almost 3.0 at 20 seconds periods. Available evidence suggests that the effective Q for 50 seconds waves lies between 100 and 200 globally, while this quantity for 20 second waves may be anywhere from 100 to over 1000 because of the extremely heterogeneous nature of the crust. The character of dispersion at 50 seconds is less variable than at 20 seconds, but equalization procedures should still be applied if oceanic and continental paths are involved. Again this could be done by calculating the stationary-phase-approximation factor or by computing spectra of the signals. Thus, at longer periods we can take advantage of more consistent behavior of surface waves over the large range of possible earth structures, thereby reducing uncertainties in M_S and yield. Also, use of longer periods which are the first-arriving wave groups may reduce concern over multiple-path effects on amplitudes. It has yet to be shown that the signal-to-noise ratio for 50-second waves from explosions can be made to exceed that for 20-second waves though.

REFERENCES

Båth, Markus, 1968, Mathematical aspects of seismology: Elsevier Publishing Co., New York.

Ben-Menahem, Ari, and Harkrider, David G., 1964, Radiation patterns of seismic surface waves from buried dipolar point sources in a flat stratified earth: J. Geophys. Res., v. 69, p. 2605-2620.

Brune, James N., 1962, Attenuation of dispersed wave trains: Bull. Seismol. Soc. Amer., v. 52, p. 109-112.

Brune, James, N., 1969, Surface waves and crustal structure: in the Earth's Crust and Upper Mantle, Ed. Pembroke J. Hart, American Geophysical Union, Washington, D. C.

Capon, J., 1970, Analysis of Rayleigh-wave multipath propagation at LASA: Bull. Seismol. Soc. Amer., v. 60, p. 1701-1732.

Eriesson, Ulf, 1971, A linear model for the yield dependence of magnitudes measured by a seismograph network: Geophys. J. R. Astr. Soc., (in press).

Evernden, Jack F., and Wilson, John, 1971, Regional dependence of surface-wave versus body-wave magnitude: J. Geophys. Res., v. 76, p. 3303-3308.

Gutenberg, B., 1945, Amplitudes of surface waves and magnitudes of shallow earthquakes: Bull. Seismol. Soc. Amer., v. 35, p. 3-12.

Harkrider, David G., 1964, Surface waves in multilayered elastic media. I. Rayleigh and Love waves from buried sources in a multilayered elastic half-space: Bull. Seismol. Soc. Amer., v. 54, p. 627-680.

Harkrider, David G., and Anderson, Don L., 1966, Surface wave energy from point sources in plane layered earth models, J. Geophys. Res., v. 71, p. 2967-2980.

Lambert, D.G., von Seggern, D.H., Alexander, S.S., and Galat, G.A., 1969, The LOCO SHOT experiment, Vol. II, Comprehensive analysis: Seismic Data Laboratory Report No. 231, Teledyne Geotech, Alexandria, Virginia.

Marshall, P.D., and Carpenter, L.W., 1966, Estimates of Q for Rayleigh waves: Geophys. J. R. Astro. Soc., v. 10, p. 549-550.

McGarr, Arthur, 1969, Amplitude variations of Rayleigh waves -- propagation across a continental margin: Bull. Seismol. Soc. Amer., v. 59, p. 1281-1306.

Molnar, Peter, Savino, John, Sykes, Lynn R., Lieberman, R.C., Wade, George, and Pomeroy, Paul W., 1969, Small earthquakes and explosions in Nester North America recorded by new high-gain, long-period seismographs: Nature, v. 221, p. 1268-1273.

Sato, Yasuo, 1960, Synthesis of dispersed waves by means of Fourier transform: Bull. Seismol. Soc. Amer., v. 50, p. 117-126.

Tryggvason, Eysteinn, 1965, Dissipation of Rayleigh wave energy, J. Geophys. Res., v. 70, p. 1449-1455.

Tsai, Yi-Ben and Aki, Keiiti, 1969, Simultaneous determination of the seismic moment and attenuation of seismic surface waves: Bull. Seismol. Soc. Amer., v. 59, p. 275-287.

von Seggern, D.H., 1969, Effects of radiation patterns on spectra and magnitude estimates: Seismic Data Laboratory Report No. 233, Teledyne Geotech, Alexandria, Virginia.

von Seggern, D.H. and Lambert, D.G., 1969, Dependence of theoretical and observed Rayleigh-wave spectra on distance, magnitude, and source type: Seismic Data Laboratory Report No. 240, Teledyne Geotech, Alexandria, Virginia.

von Seggern, D.H., 1970, Surface-wave amplitude-versus-distance relation in the Western United States: Seismic Data Laboratory Report No. 249, Teledyne Geotech, Alexandria, Virginia.

TABLE I

Phase Velocities Taken From Brune (1969) and Used in the Seismogram Synthesis of this Report

Shield		Mid-Continent		Basin-Range		Alpine		Great Island Arc		Deep Ocean	
T(sec)	C(km/sec)										
100*	4.17	100*	4.01	100*	4.00	100*	3.92	100*	3.90	100*	3.97
60	4.17	50	4.00	50*	3.96	50*	3.90	60	3.88	36	3.98
50	4.13	40	3.96	40	3.81	40	3.81	50	3.85	28	4.00
40	4.08	30	3.80	30	3.62	30	3.62	40	3.81	25	4.02
30	3.93	26	3.70	20	3.40	20	3.37	30	3.69	22	4.00
20	3.67	22	3.57	15*	3.27	15	3.27	26	3.62	20	3.98
16	3.52	18	3.40	10*	3.15	12	3.20	22	3.52	18	3.90
12	3.39	14	3.26	7*	3.05	10*	3.15	18*	3.40	16	3.80
10	3.35	10	3.15	5*	2.90	7*	3.05	14*	3.28	14*	3.64
5	3.25	7*	3.00			5*	2.95	10*	3.14	12*	3.35
		5*	2.90					7*	3.00	10*	2.80
								5*	2.88	8*	2.50
										6*	2.20
										5*	2.00

*Extrapolated values

TABLE II

Values of Q (Tsai and Aki, 1969) and Values of the Medium Response for a Gutenberg Continental Earth Model (Ben-Menahem and Harkrider, 1964) used in the Seismogram Synthesis of this Report

Period	Q	Period	$\varepsilon_o A_R k^{1/2}$
100	130	100	4.96
50	130	50	15.1
40	200	40	23.1
33	300	30	45.4
29	600	20	123.
25	900	10	350.
20	700	5	910.
18	500		
15	300		
10	200		
5	100		

TABLE III

Summary of Procedure for Amplitude Equalization
of Twenty-Second Period Waves at 10,000 km
Using the Stationary-Phase Approximation Factor

Crustal Type	Measured Amplitude	U	dU/dT	$(dU/dT)^{1/2}$	$\frac{U}{(dU/dT)^{1/2}}$	Equalized + Amplitude
Shield	75.6	3.08	.030	.173	17.8	4.25
Mid-continent	43.2	2.82	.037	.192	14.7	2.94
Basin-range	45.8	2.81	.060	.245	11.5	3.98
Alpine	34.9	2.68	.048	.219	12.2	2.89
*Great Island arc	65.0	2.96	.040	.200	14.8	4.39
Deep Ocean	18.1	3.59	.250	.500	7.18	2.52

*All quantities for Great Island Arc structure are given at T = 21 sec.; for the other structures at T = 20 sec.

+Equalized amplitude is equal to the measured amplitude divided by $U(dU/dT)^{-1/2}$

TABLE IV

Relative System Magnification for LRSM Long-Period Recordings

Period (sec)	Relative System Magnification
8	.100
9	.138
10	.188
11	.245
12	.310
13	.390
14	.480
15	.580
16	.690
17	.790
18	.880
19	.920
20	.960
21	.970
22	.980
23	.990
24	.995
25	1.000
26	.990
27	.960
28	.920

TABLE V

Maximum Amplitudes and Corresponding Periods
Measured on the Synthetic Seismograms of
Figures 5a, 5b and 5c

Structure \ Distance (km)	100	200	400	600	800	1000	1300	1600	2000	3000	4000	6000	8000	10,000
Shield	1750* / 11*	1500 / 11	287 / 16	211 / 16	170 / 16	148 / 16	115 / 16	98.4 / 16	76.0 / 16	50.0 / 16	29.7 / 17	16.8 / 17	9.92 / 19	7.85 / 19
Mid-Continent	2450 / 10	1790 / 10	541 / 15	458 / 12	410 / 12	221 / 14	167 / 14	109 / 15	76.3 / 16	42.6 / 16	25.8 / 18	14.0 / 18	8.16 / 20	6.56 / 20
Basin-Range	2510 / 10	1680 / 10	845 / 11	405 / 13	254 / 14	225 / 14	159 / 15	131 / 15	87.7 / 16	46.9 / 17	34.2 / 17	19.2 / 18	11.4 / 19	8.16 / 19
Alpine	2480 / 10	1720 / 10	855 / 11	458 / 14	221 / 15	258 / 14	150 / 15	134 / 15	101 / 15	56.9 / 16	34.4 / 17	15.2 / 17	9.55 / 20	6.96 / 21
Island Arc	2510 / 10	1840 / 10	459 / 14	369 / 15	177 / 16	145 / 16	134 / 15	91.7 / 16	73.3 / 16	46.5 / 16	27.9 / 17	13.6 / 19	9.95 / 19	7.98 / 20
Oceanic	597 / 15	260 / 1-	122 / 20	82.3 / 20	60.6 / 23	48.6 / 24	39.2 / 24	34.3 / 25	29.5 / 25	25.2 / 24	17.8 / 24	12.5 / 26	8.98 / 27	8.00 / 25
High-Q Mid-Continent	2500 / 10	1850 / 10	715 / 12	795 / 10	442 / 12	244 / 14	190 / 14	152 / 14	106 / 15	61.2 / 15	41.7 / 15	23.2 / 16	13.6 / 16	9.90 / 1-

*Amplitude is the maximum peak-to-peak excursion corrected for system response used in synthesis

-Period is for cycle of measured maximum amplitude

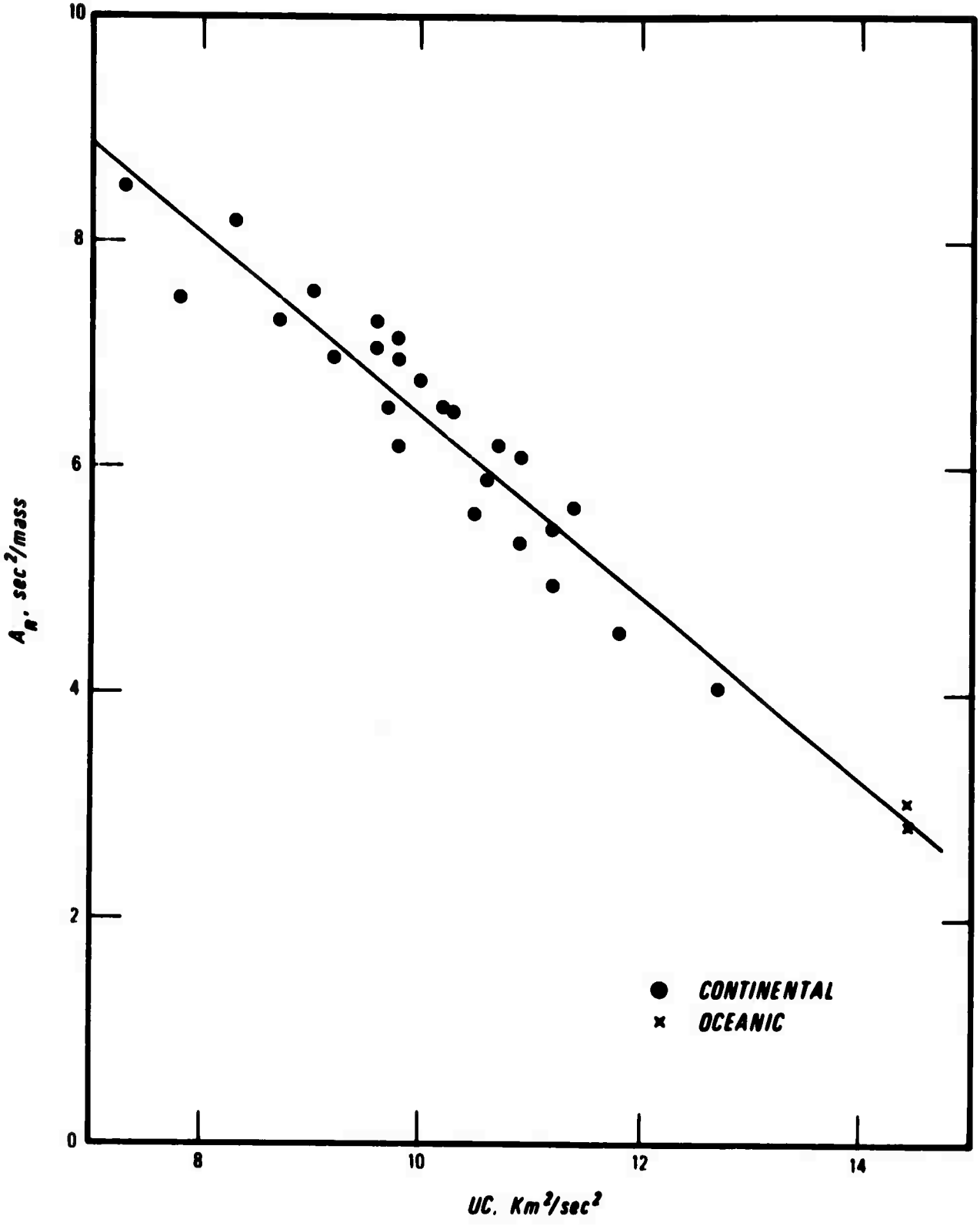

Figure 1. Relation of the Rayleigh-wave amplitude response factor to the product of group and phase velocity (twenty-second period of the fundamental mode) for various earth structures.

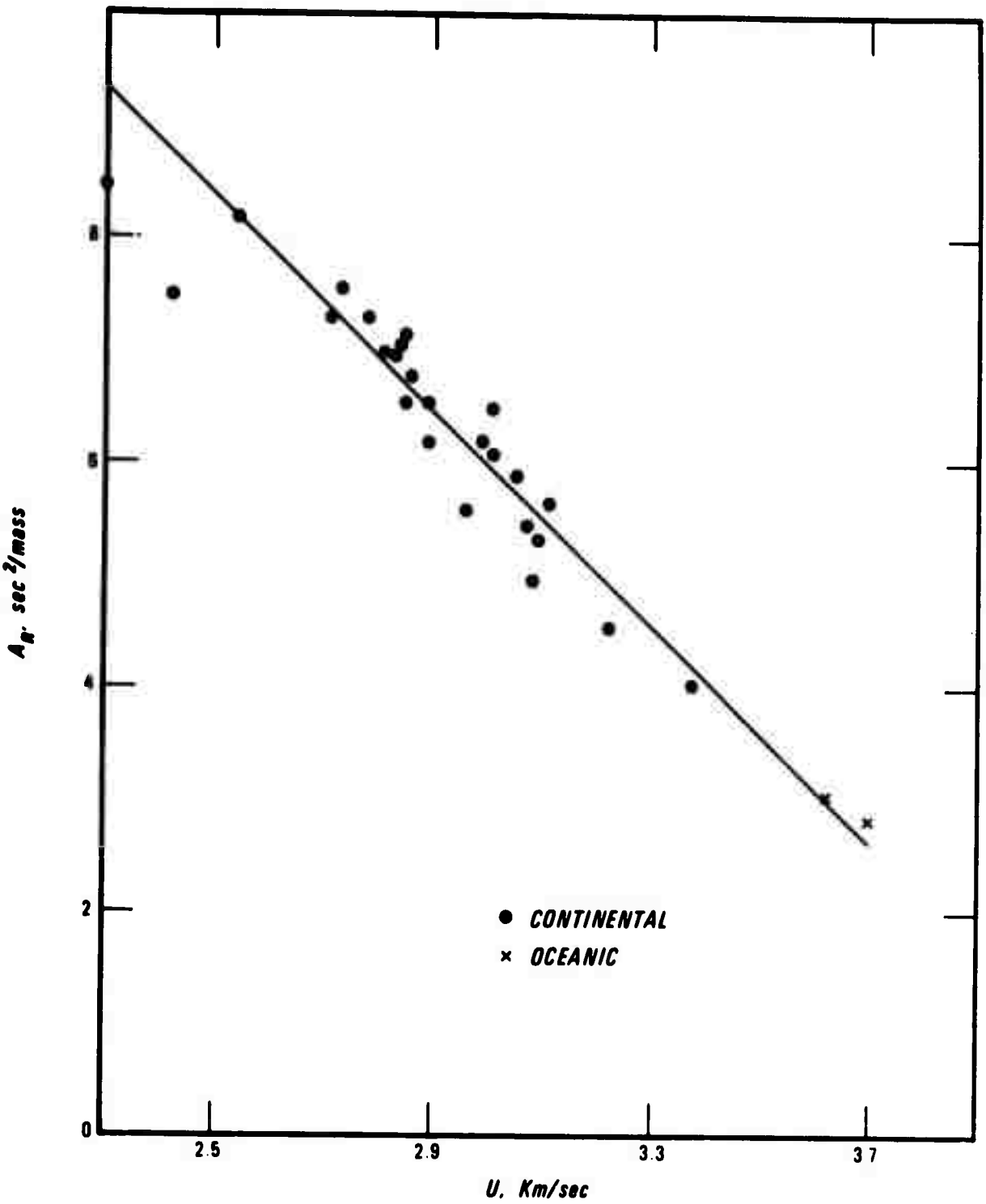

Figure 2. Relation of the Rayleigh-wave amplitude response factor to group velocity (twenty-second period of the fundamental mode) for the same earth structures as in Figure 1.

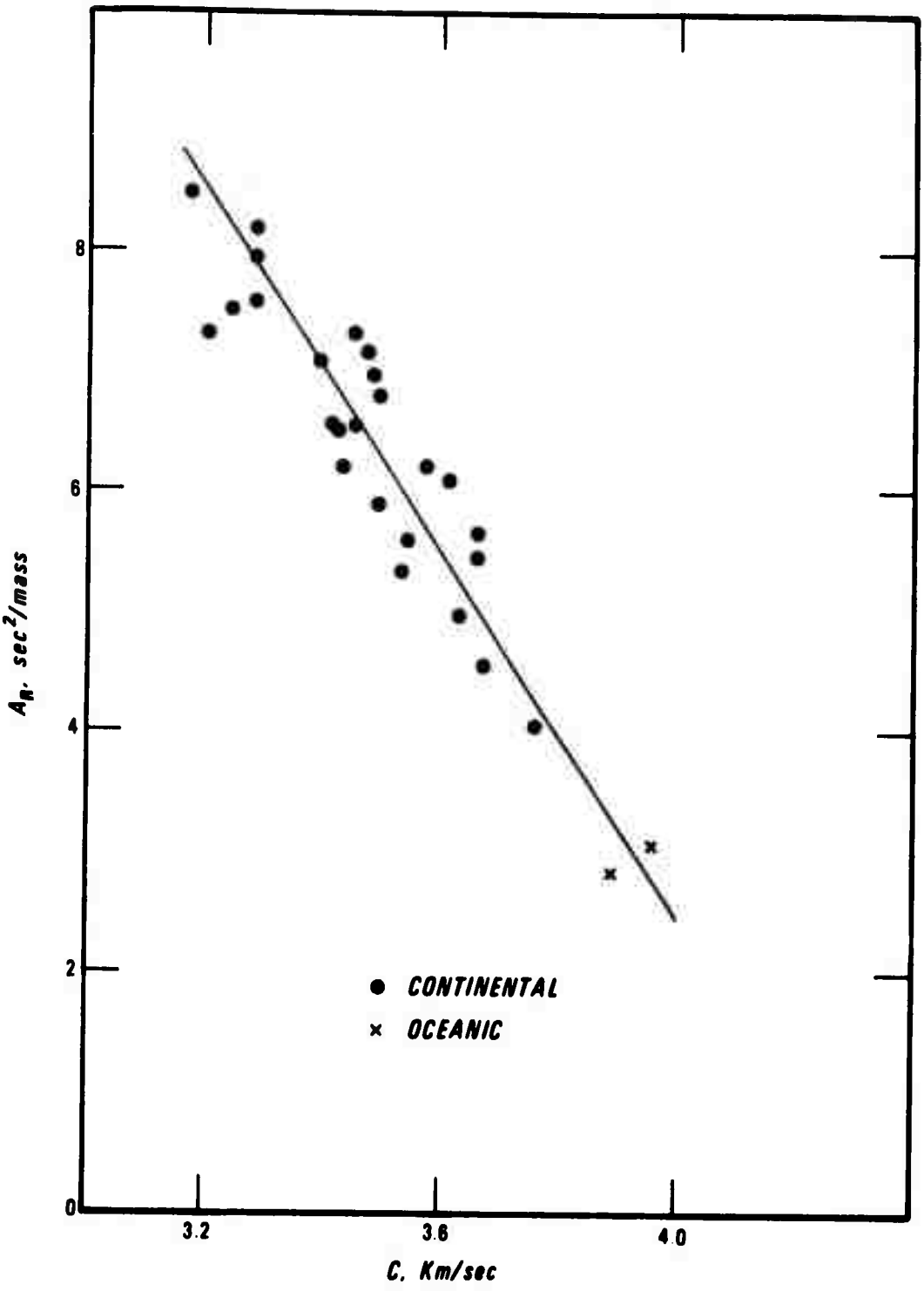

Figure 3. Relation of the Rayleigh-wave amplitude response factor to phase velocity (twenty-second period of the fumdamental mode) for the same earth structures as in Figure 1.

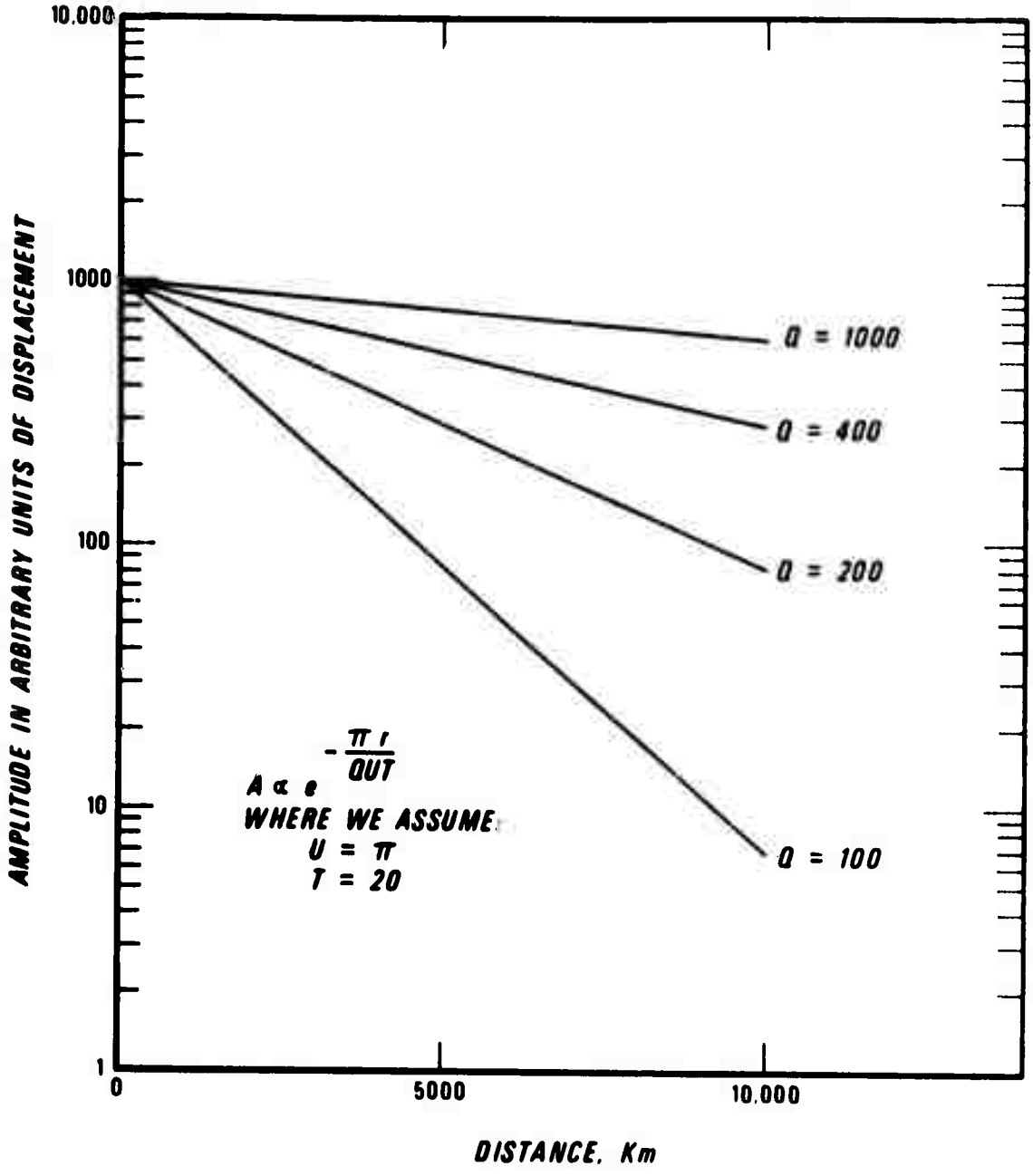

Figure 4. Amplitude-distance relation of surface waves for various values of Q.

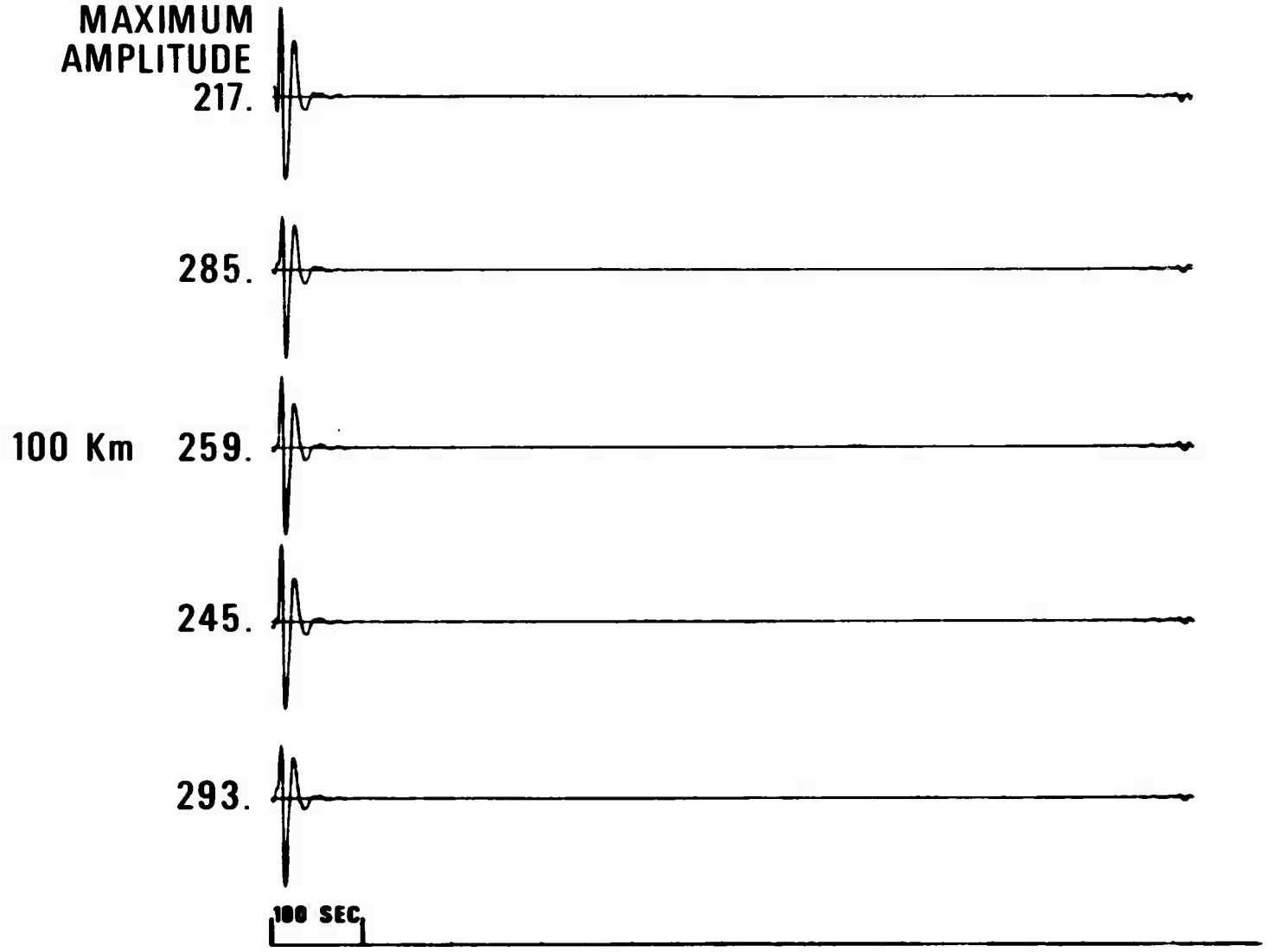

Figure 5a. Synthetic fundamental-mode Rayleigh-wave signals for five different continental structures at various epicentral distances.

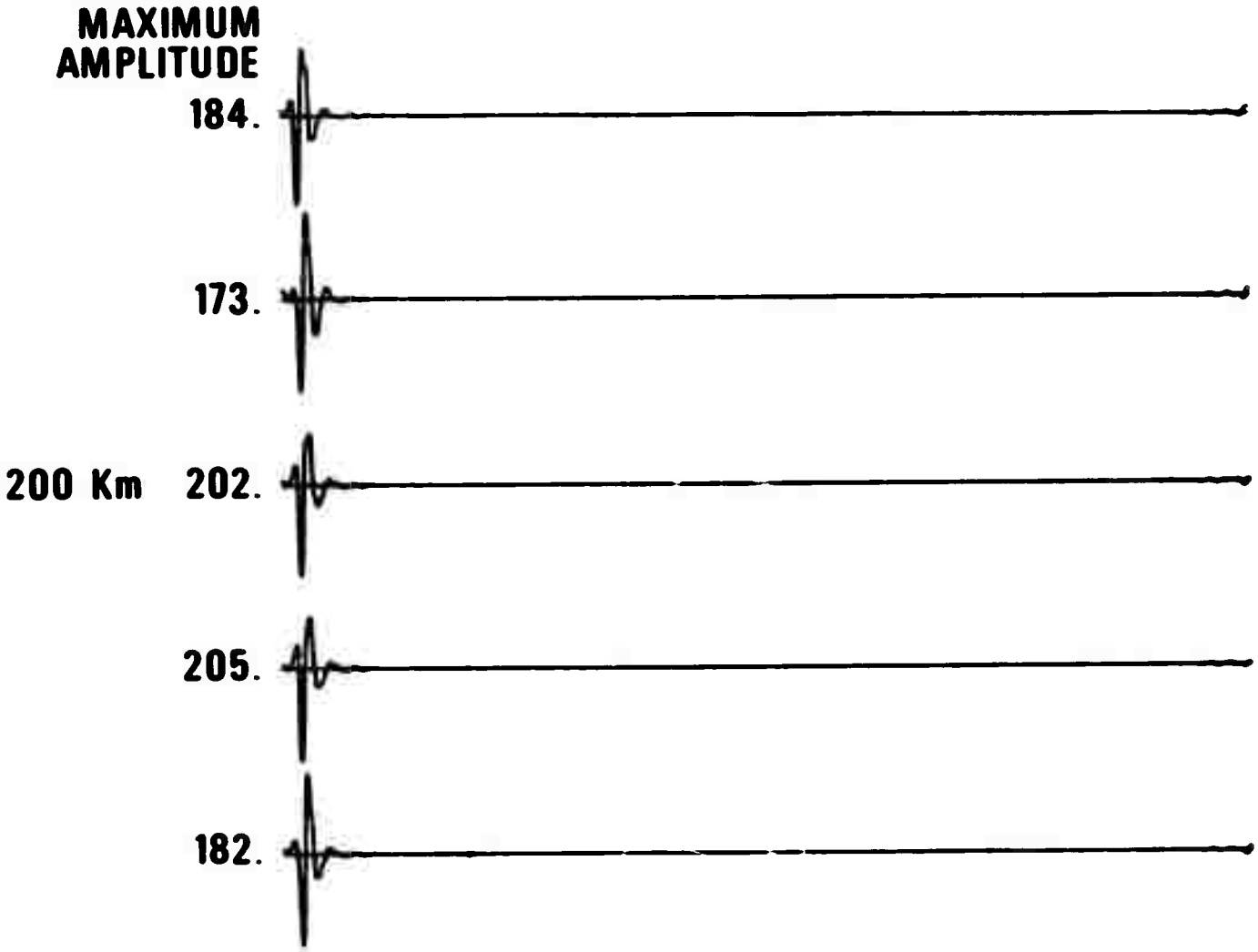

Figure 5a (cont'd.). Synthetic fundamental-mode Rayleigh-wave signals for five different continental structures at various epicentral distances.

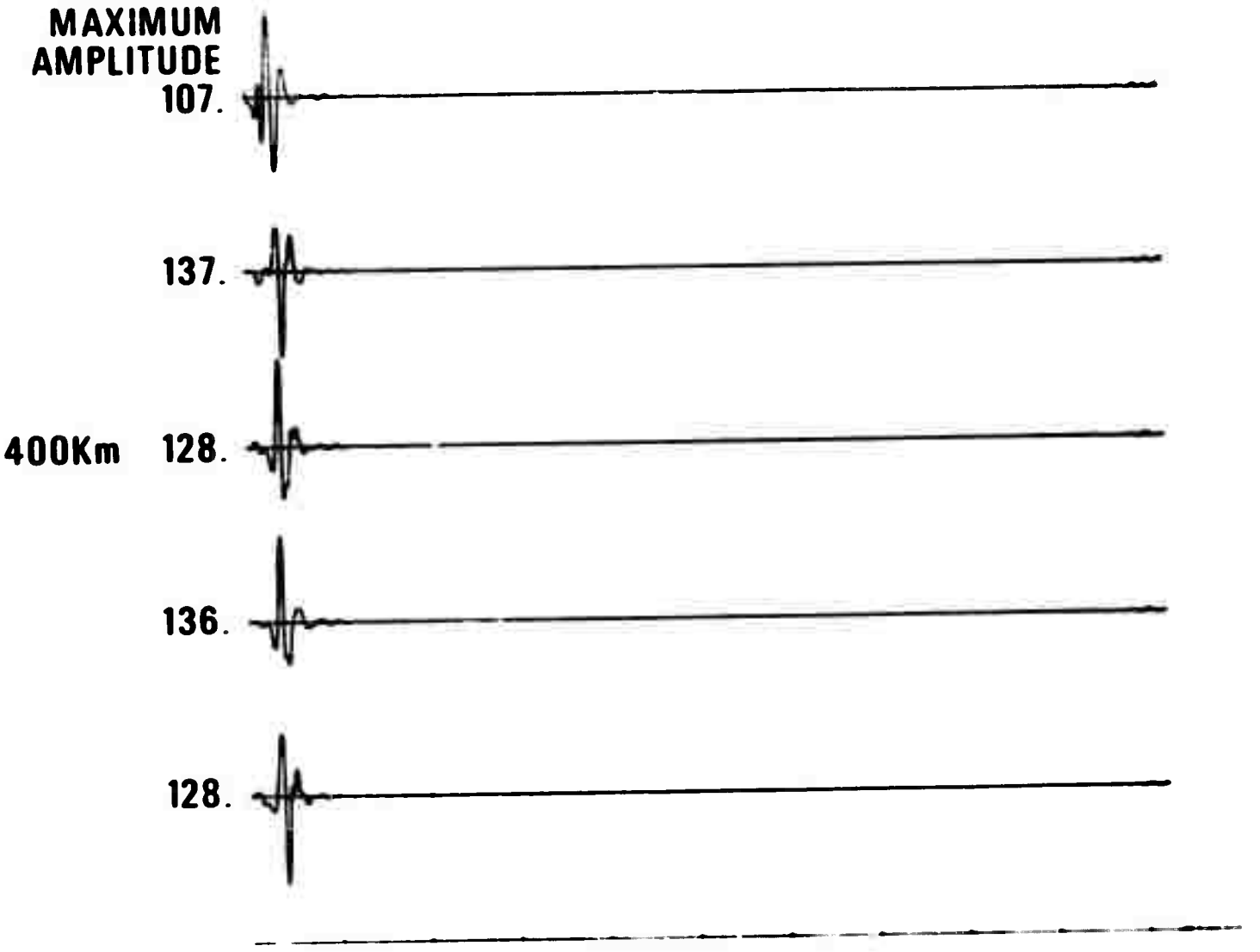

Figure 5a (cont'd.). Synthetic fundamental-mode Rayleigh-wave signals for five different continental structures at various epicentral distances.

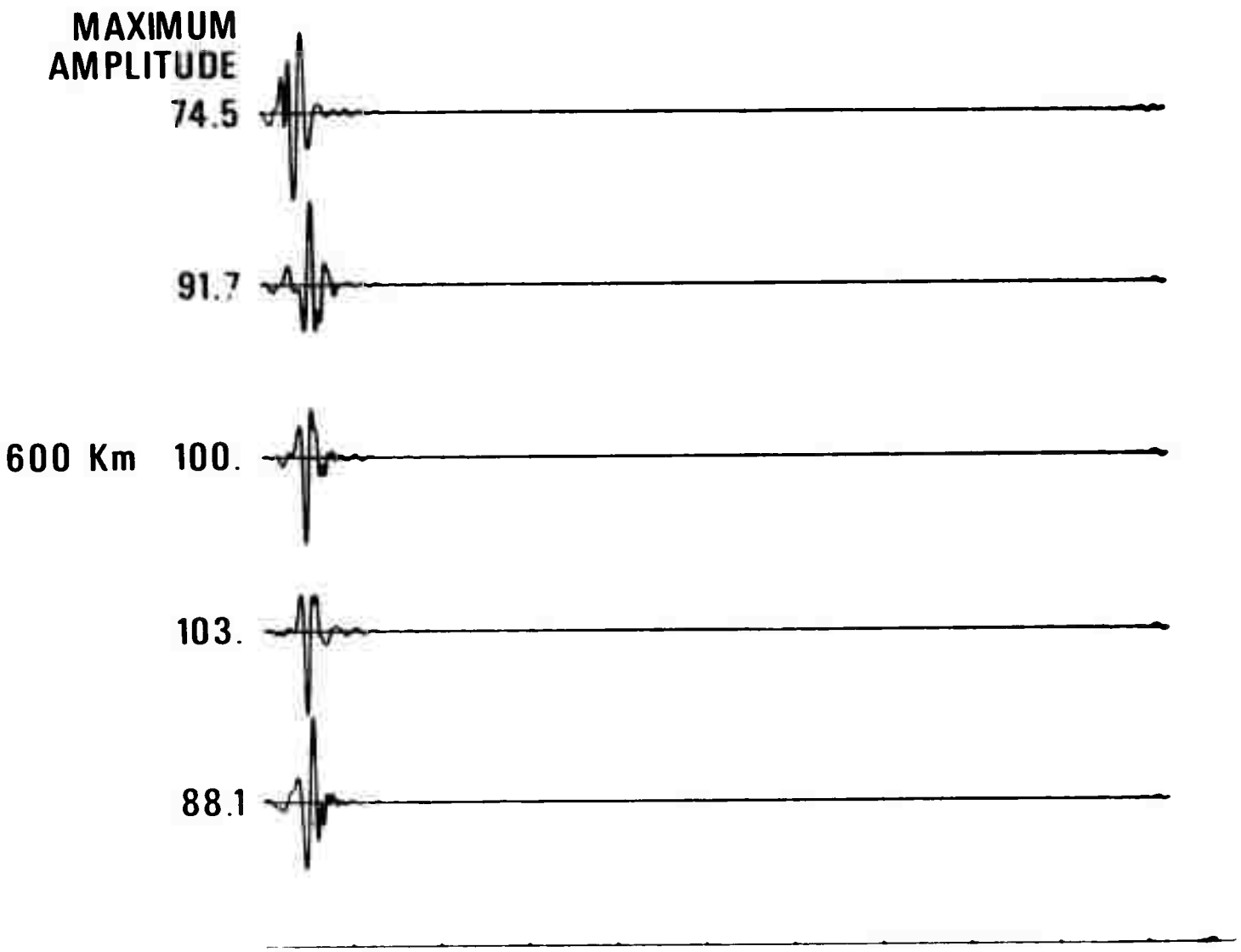

hh

Figure 5a (cont'd.). Synthetic fundamental-mode Rayleigh-wave signals for five different continental structures at various epicentral distances.

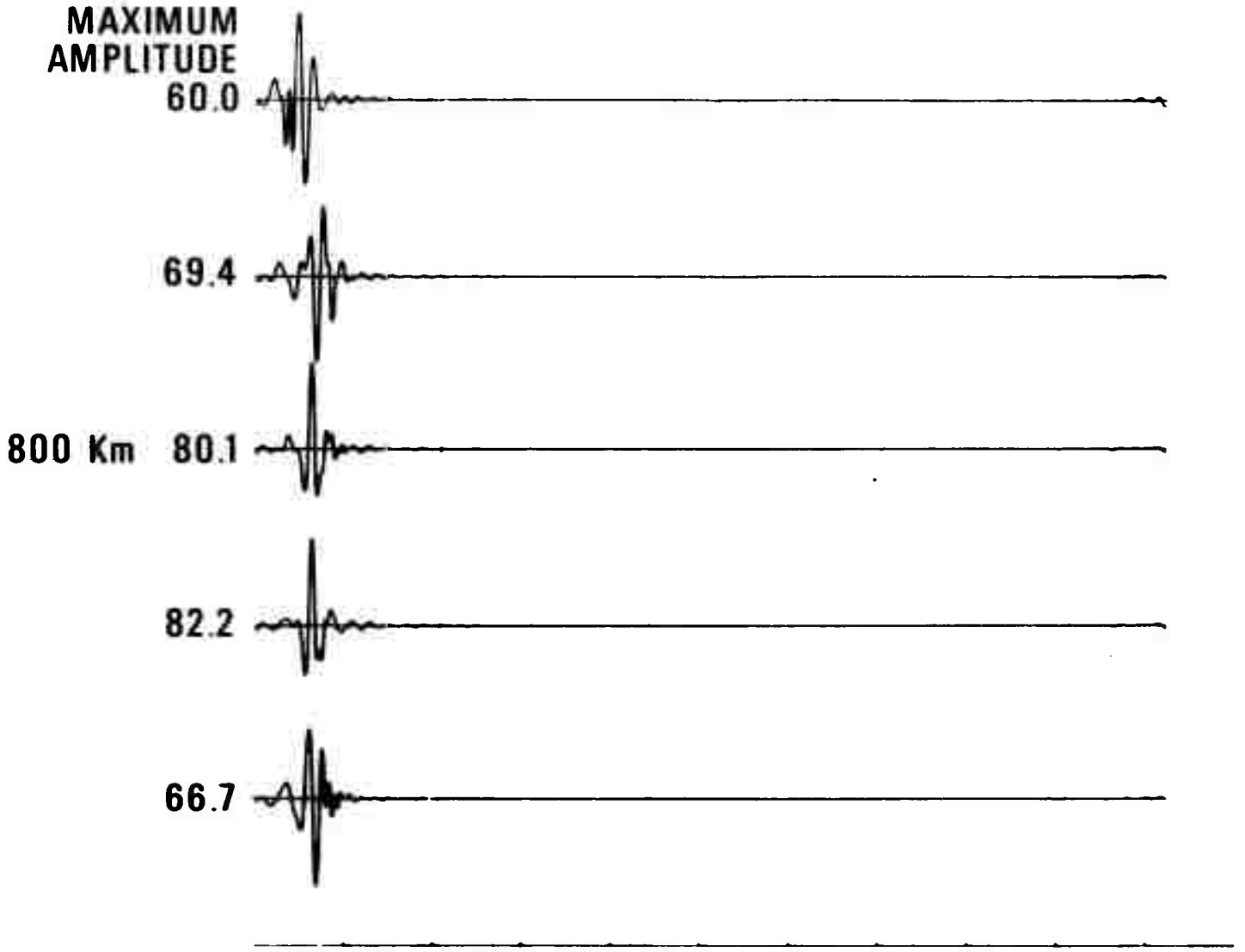

Figure 5a (cont'd.). Synthetic fundamental-mode Rayleigh-wave signals for five different continental structures at various epicentral distances.

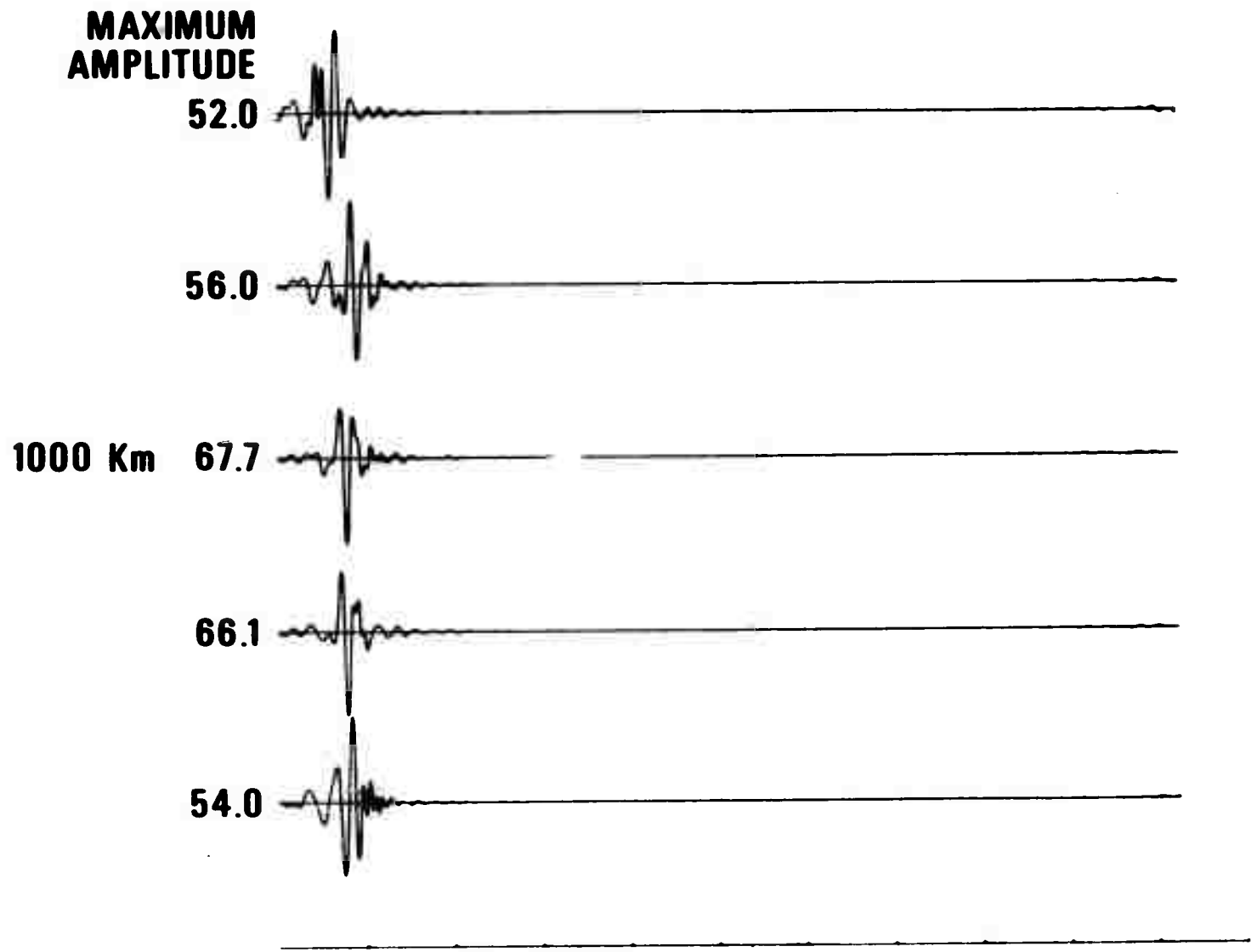

Figure 5a (cont'd.). Synthetic fundamental-mode Rayleigh-wave signals for five different continental structures at various epicentral distances.

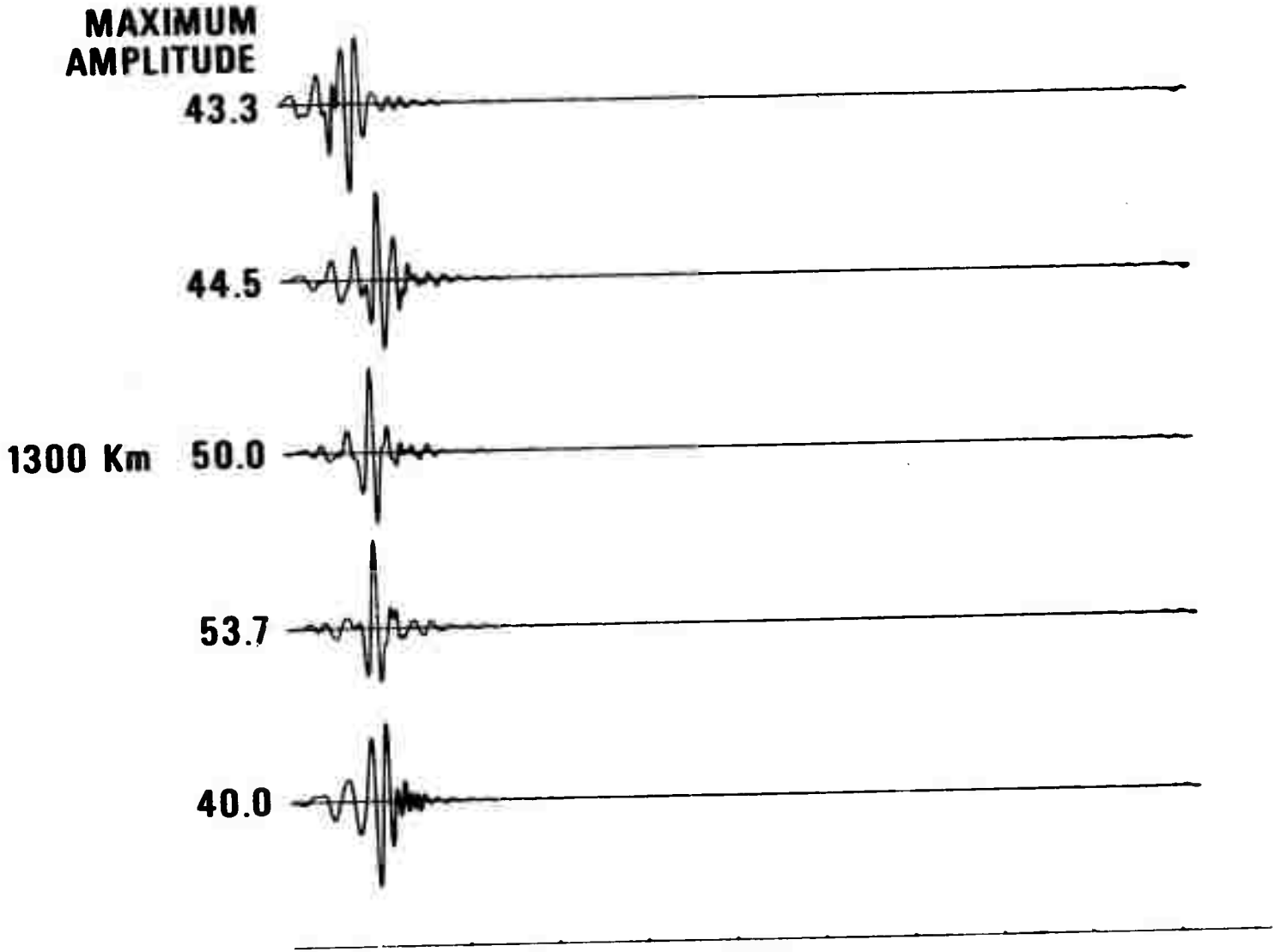

Figure 5a (cont'd.). Synthetic fundamental-mode Rayleigh-wave signals for five different continental structures at various epicentral distances.

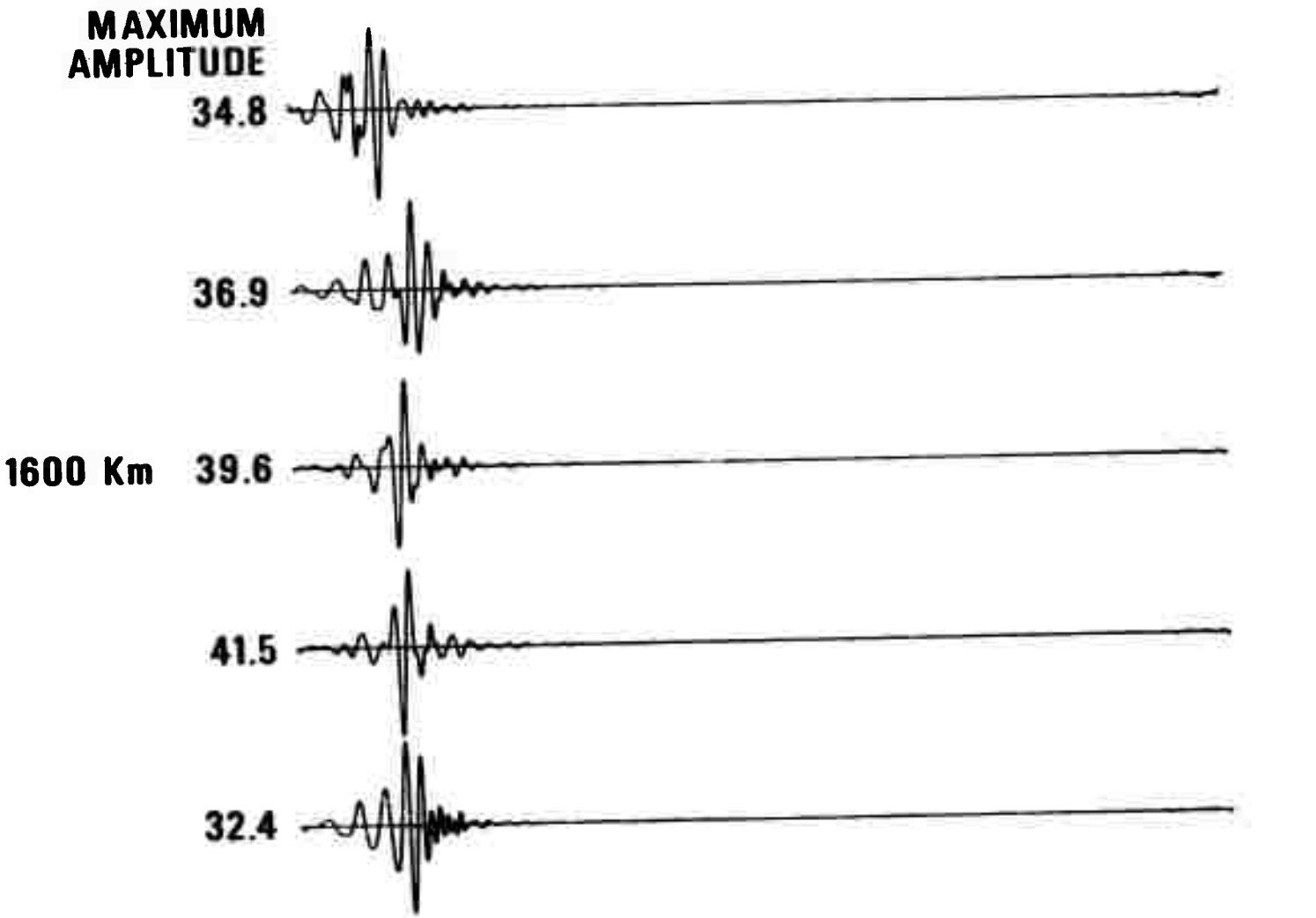

Figure 5a (cont'd.). Synthetic fundamental-mode Rayleigh-wave signals for five different continental structures at various epicentral distances.

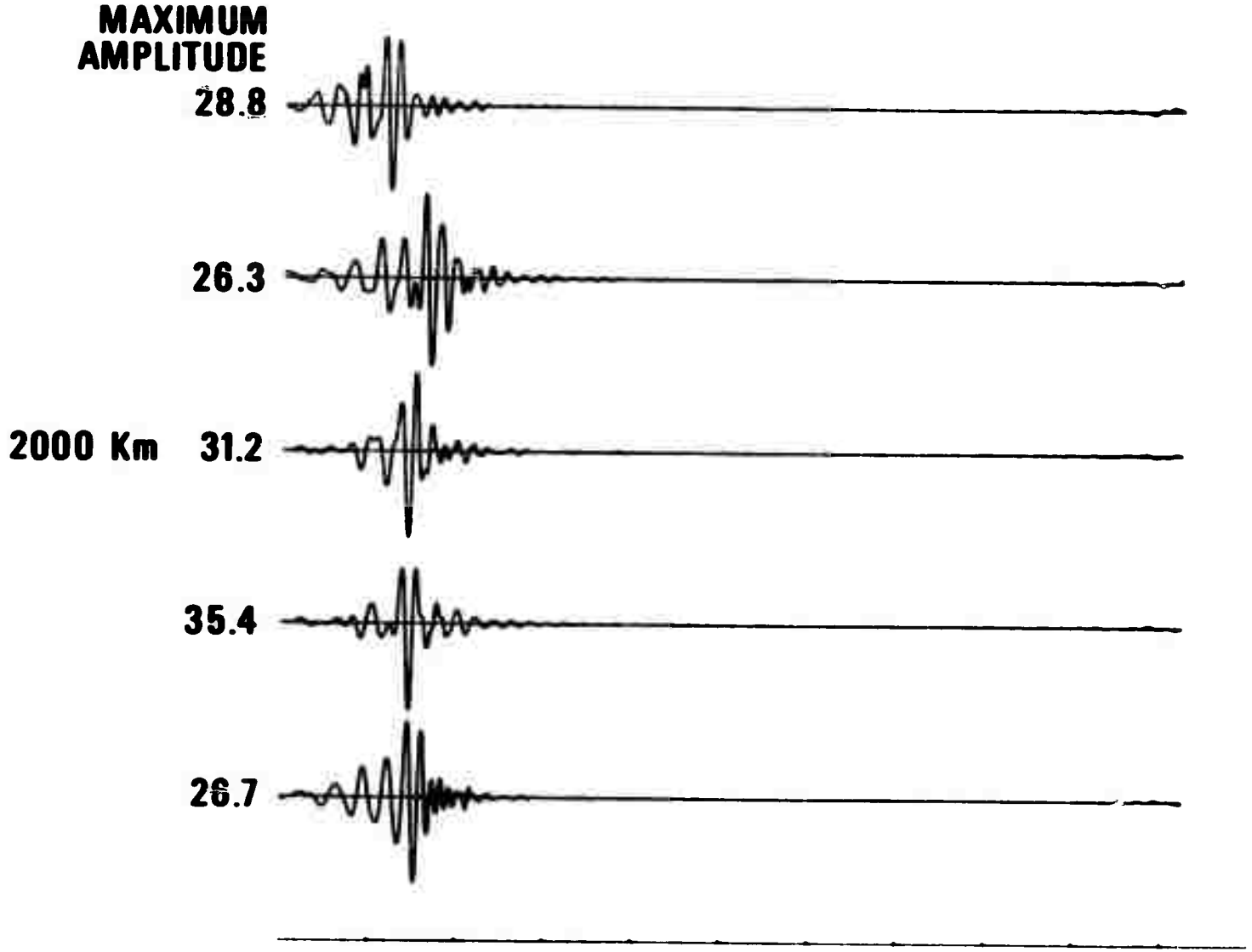

Figure 5a (cont'd.). Synthetic fundamental-mode Rayleigh-wave signals for five different continental structures at various epicentral distances.

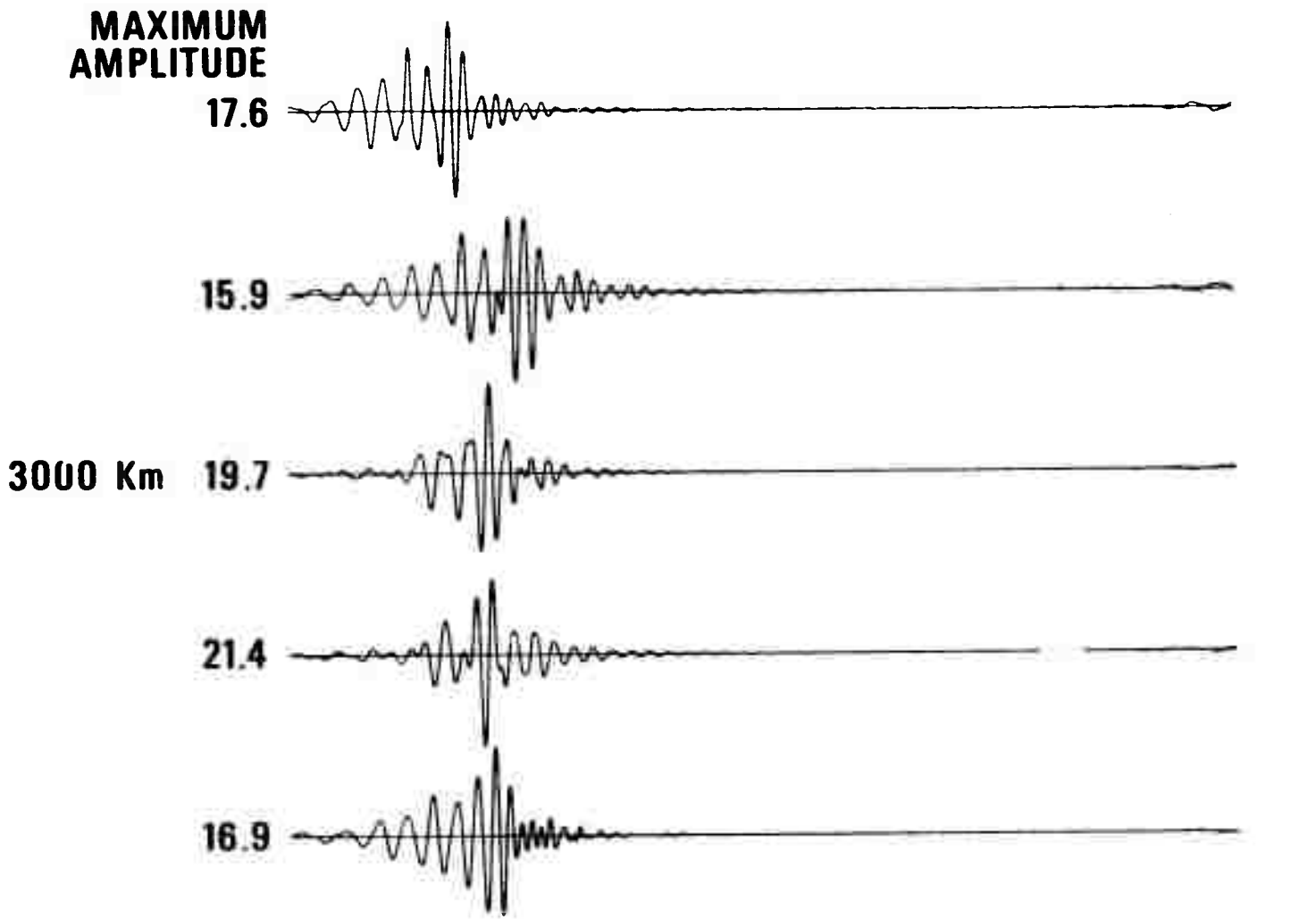

Figure 5a (cont'd.). Synthetic fundamental-mode Rayleigh-wave signals for five different continental structures at various epicentral distances.

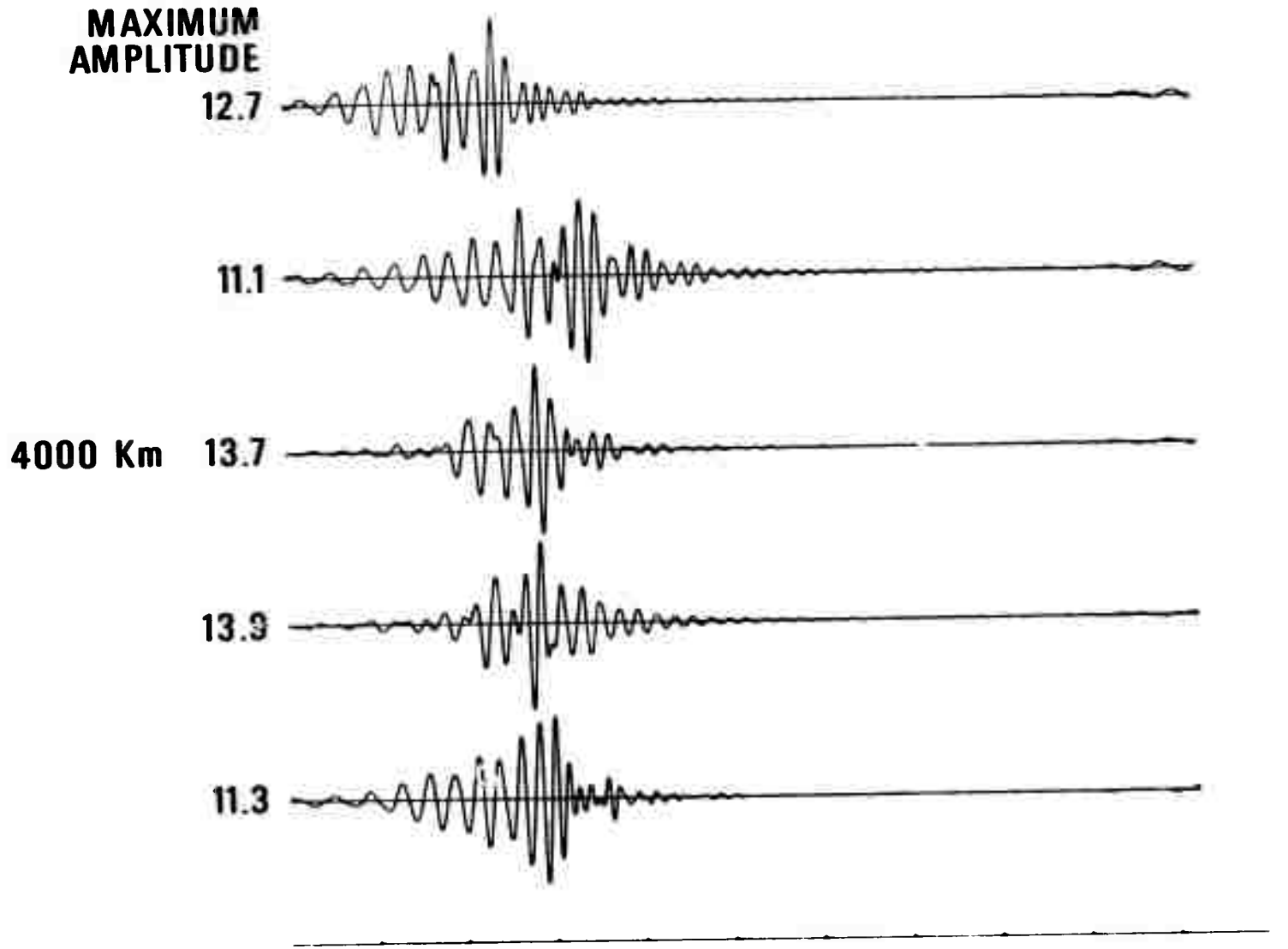

Figure 5a (cont'd.). Synthetic fundamental-mode Rayleigh-wave signals for five different continental structures at various epicentral distances.

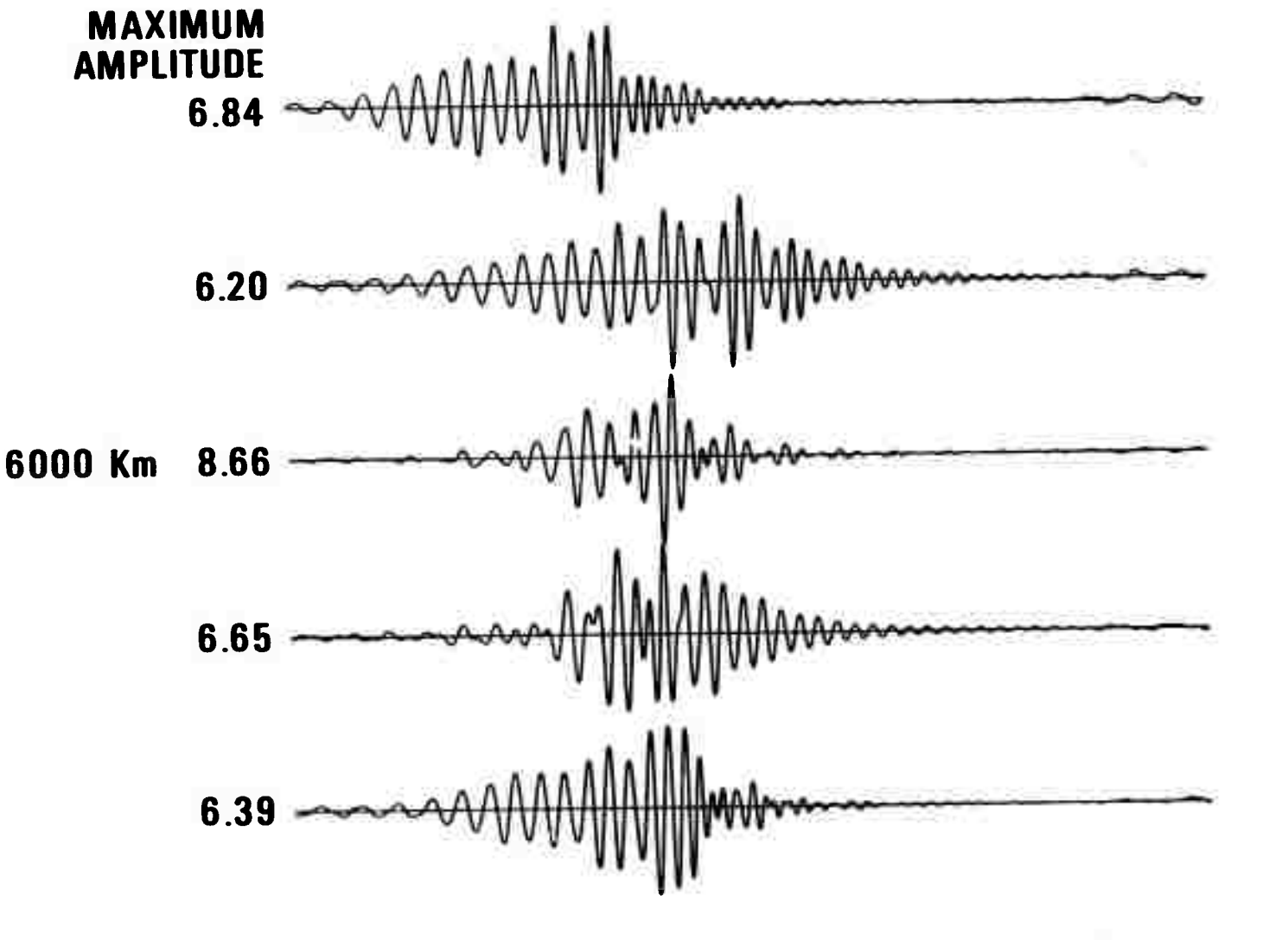

Figure 5a (cont'd.). Synthetic fundamental-mode Rayleigh-wave signals for five different continental structures at various epicentral distances.

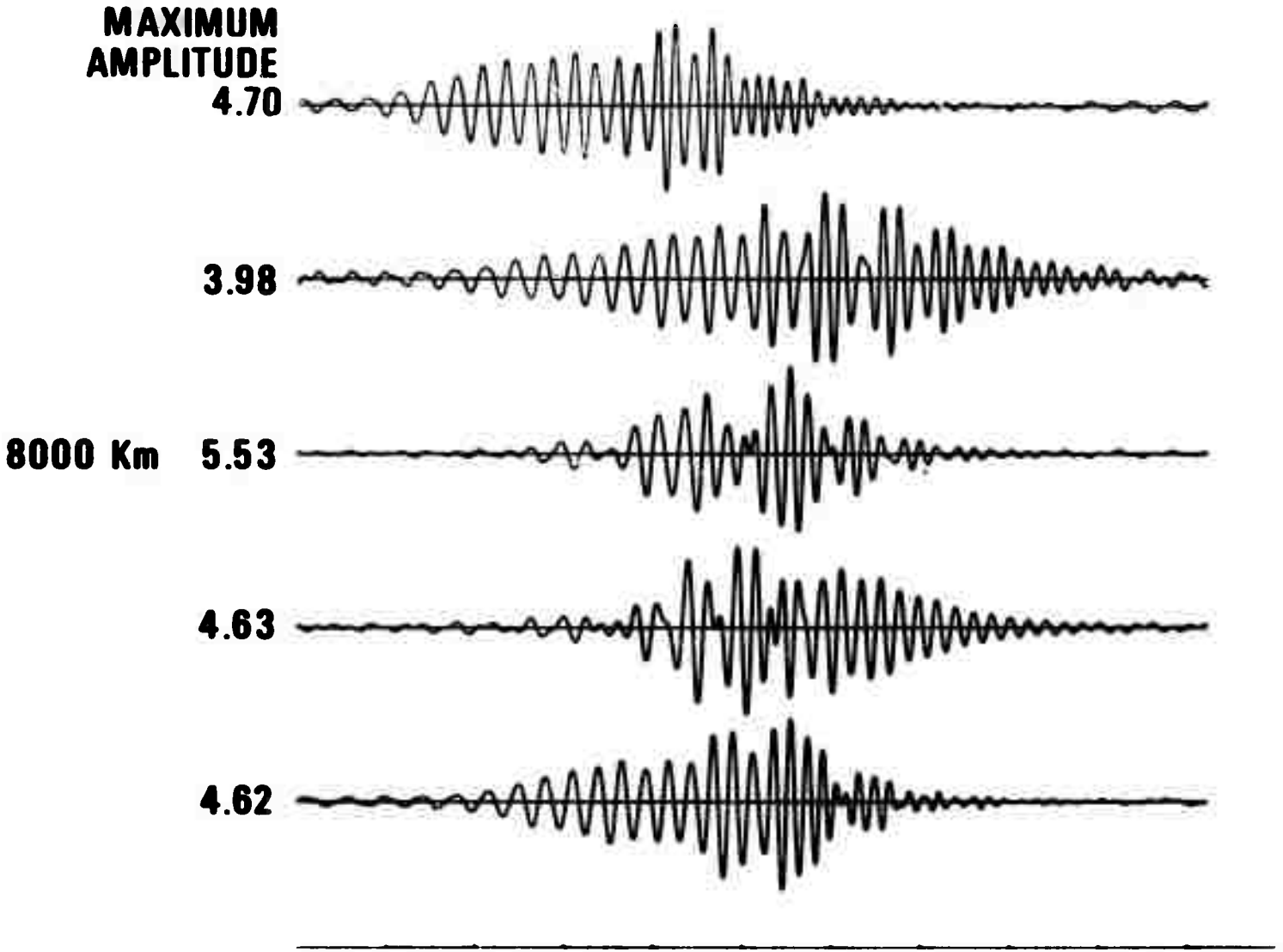

Figure 5a (cont'd.). Synthetic fundamental-mode Rayleigh-wave signals for five different continental structures at various epicentral distances.

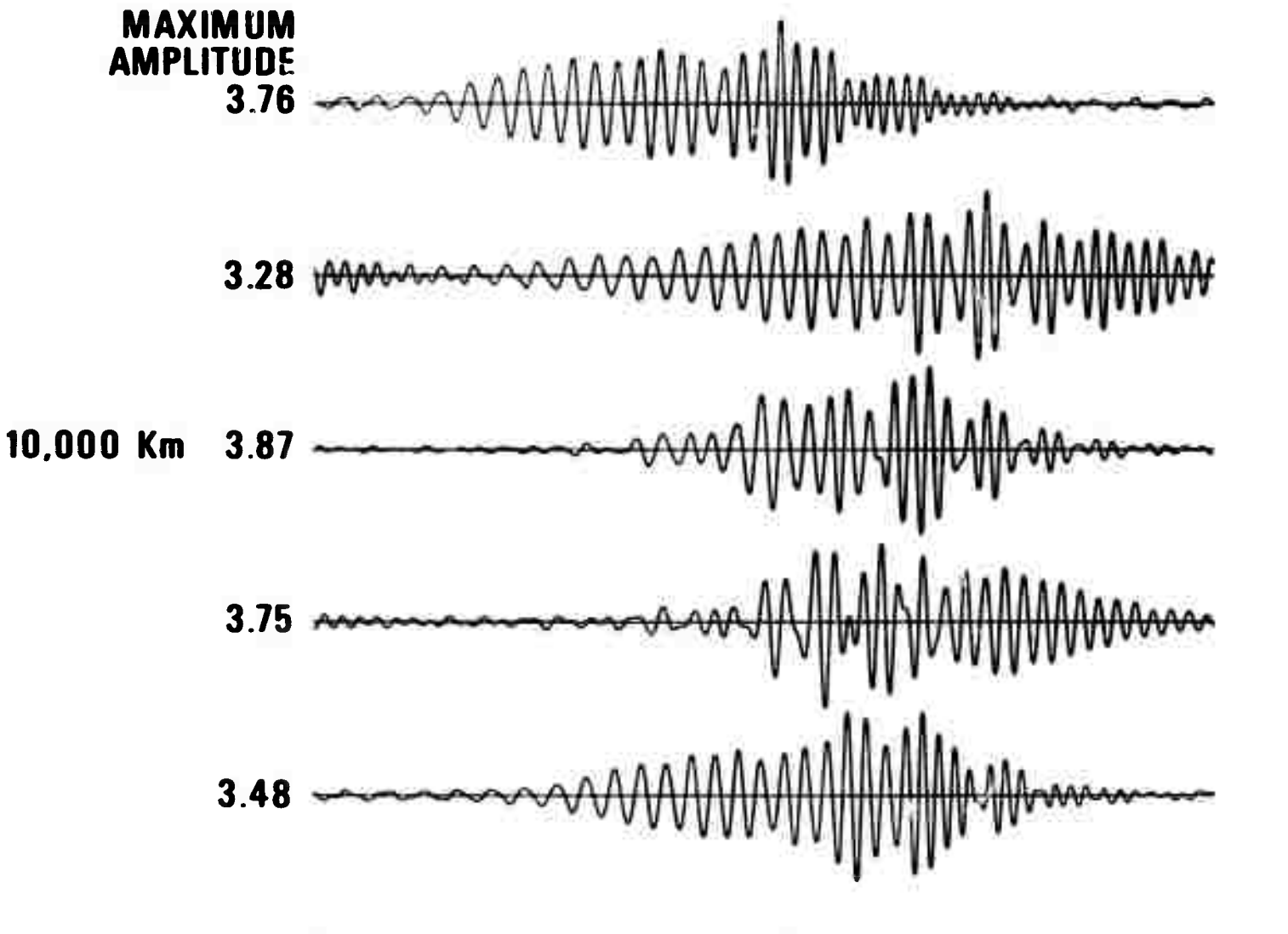

Figure 5a (cont'd.). Synthetic fundamental-mode Rayleigh-wave signals for five different continental structures at various epicentral distances.

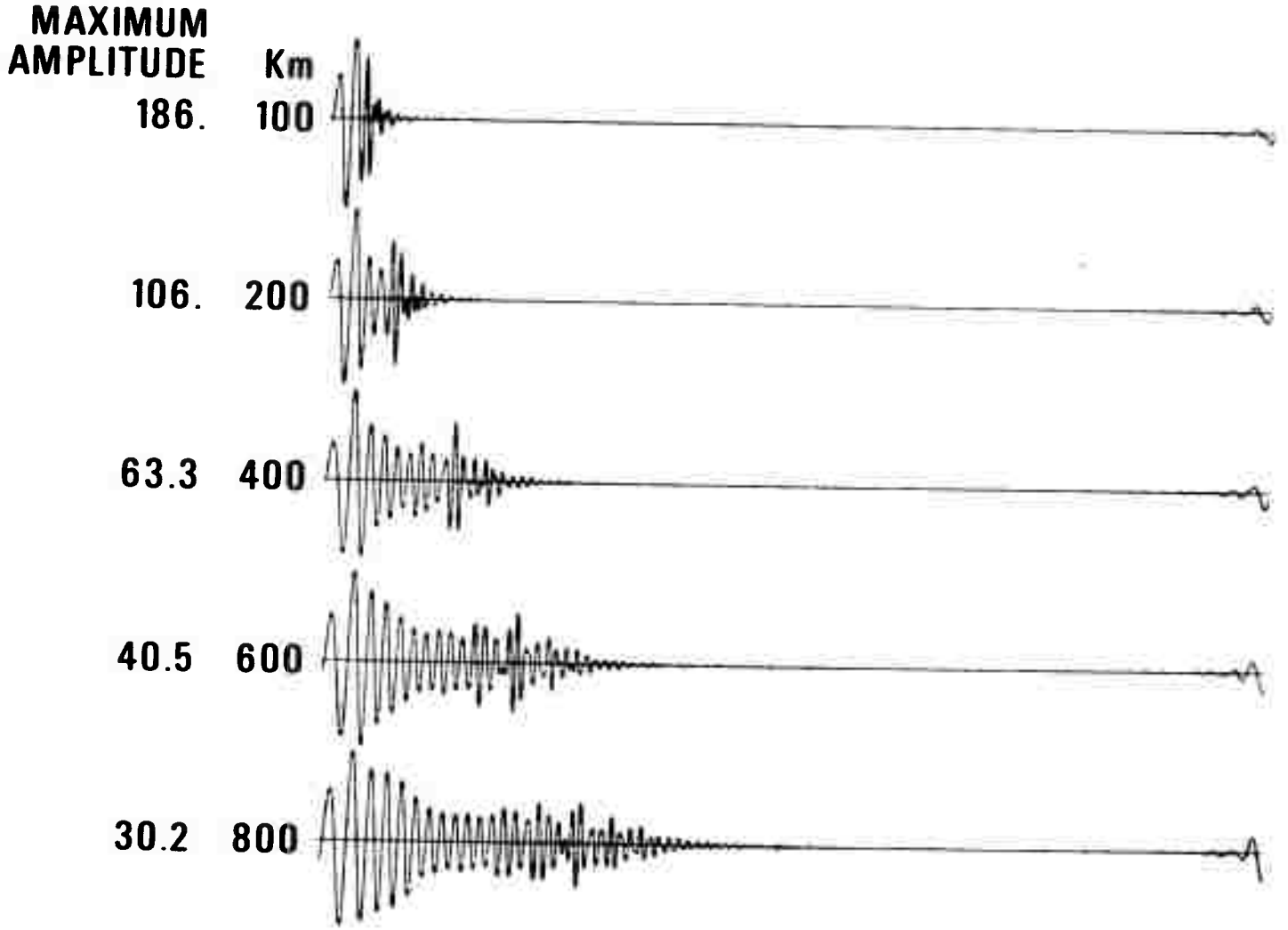

Figure 5b. Synthetic fundamental-mode Rayleigh-wave signals for a deep ocean structure at various epicentral distances.

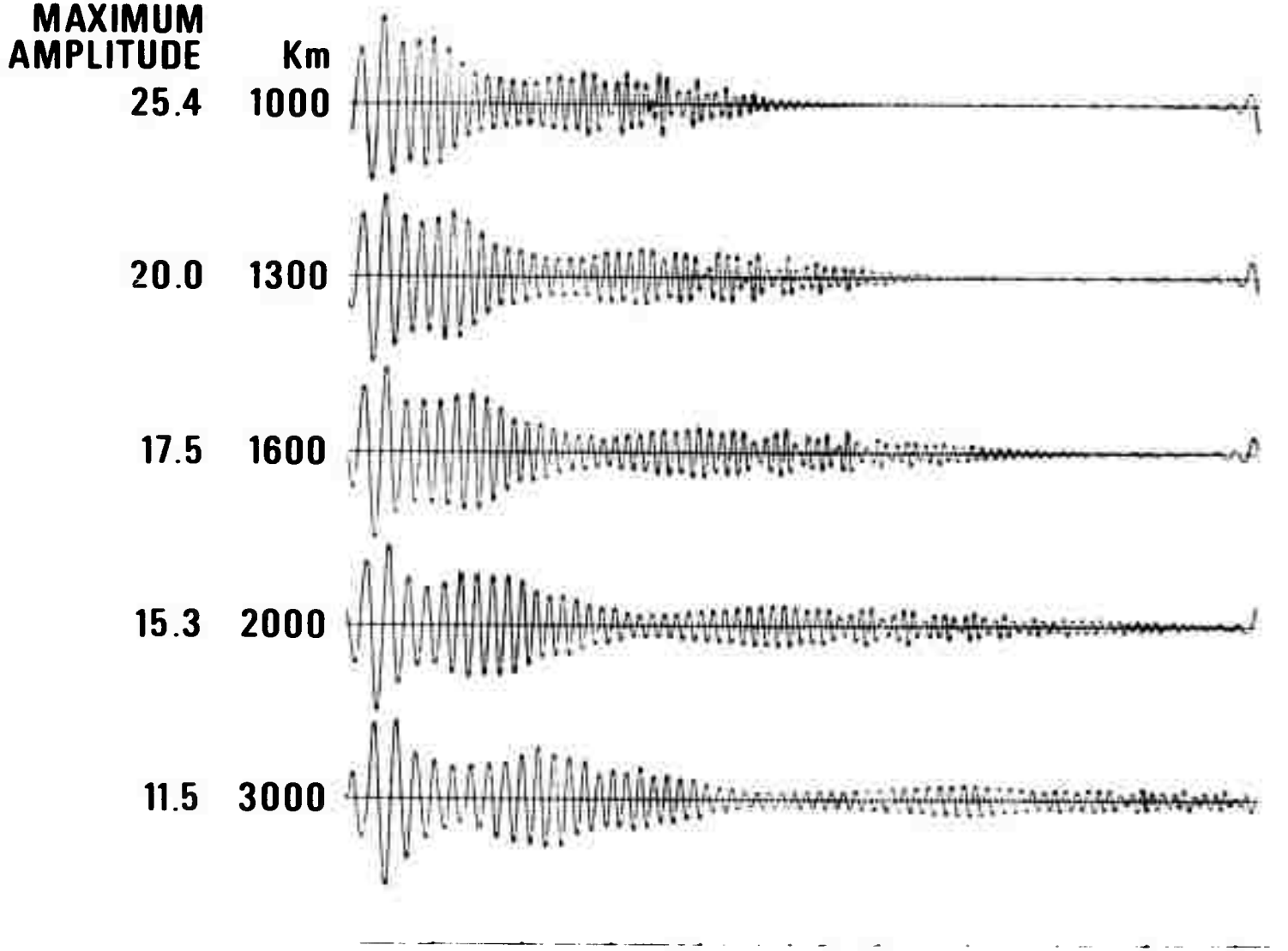

Figure 5b (cont'd.). Synthetic fundamental-mode Rayleigh wave signals for a deep ocean structure at various epicentral distances.

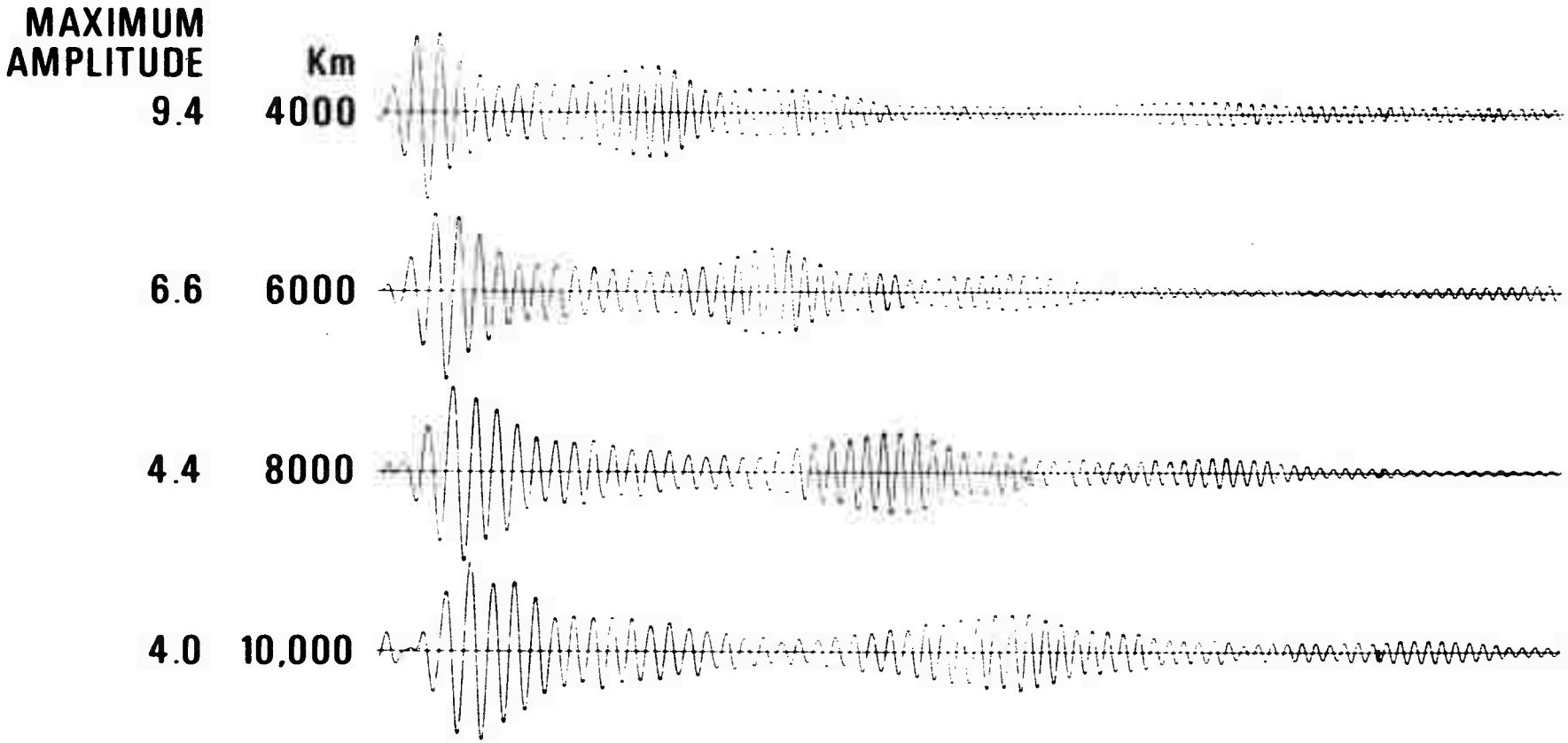

Figure 5b (cont'd.). Synthetic fundamental-mode Rayleigh wave signals for a deep ocean structure at various epicentral distances.

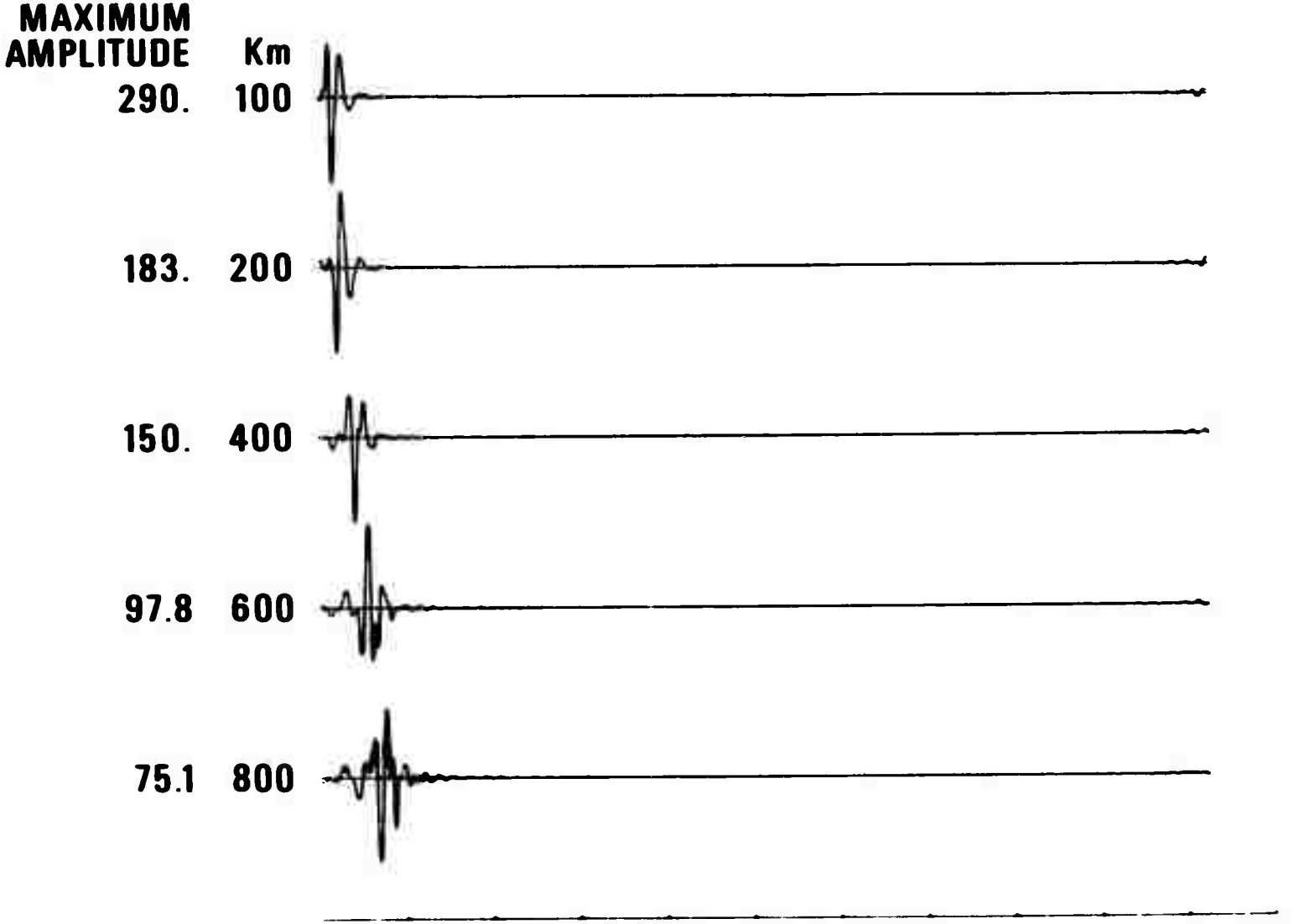

Figure 5c. Synthetic fundamental-mode Rayleigh-wave signals for a high-Q mid-continental structure at various epicentral distances.

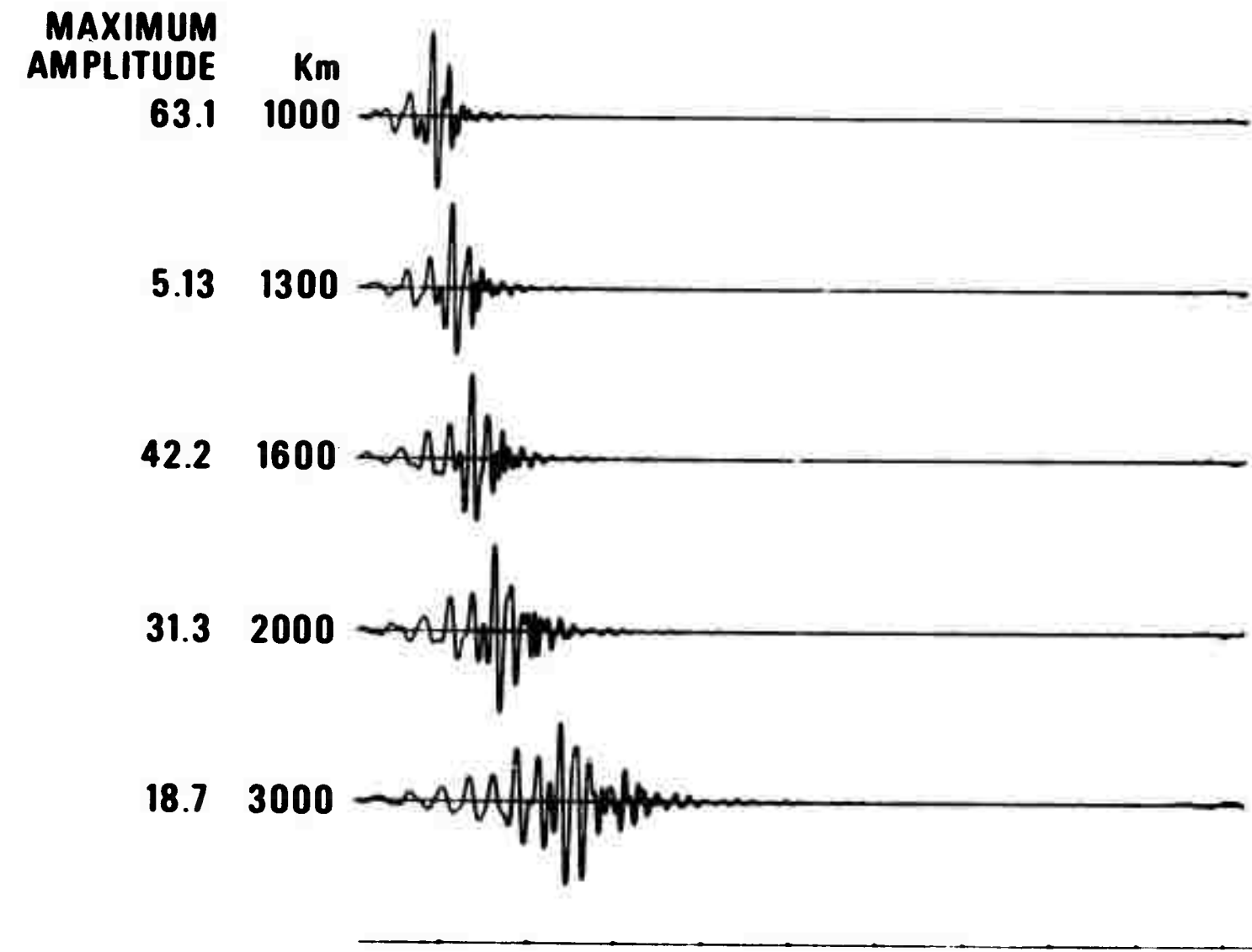

Figure 5c (cont'd.). Synthetic fundamental-mode Rayleigh-wave signals for a high-Q mid-continental structure at various epicentral distances.

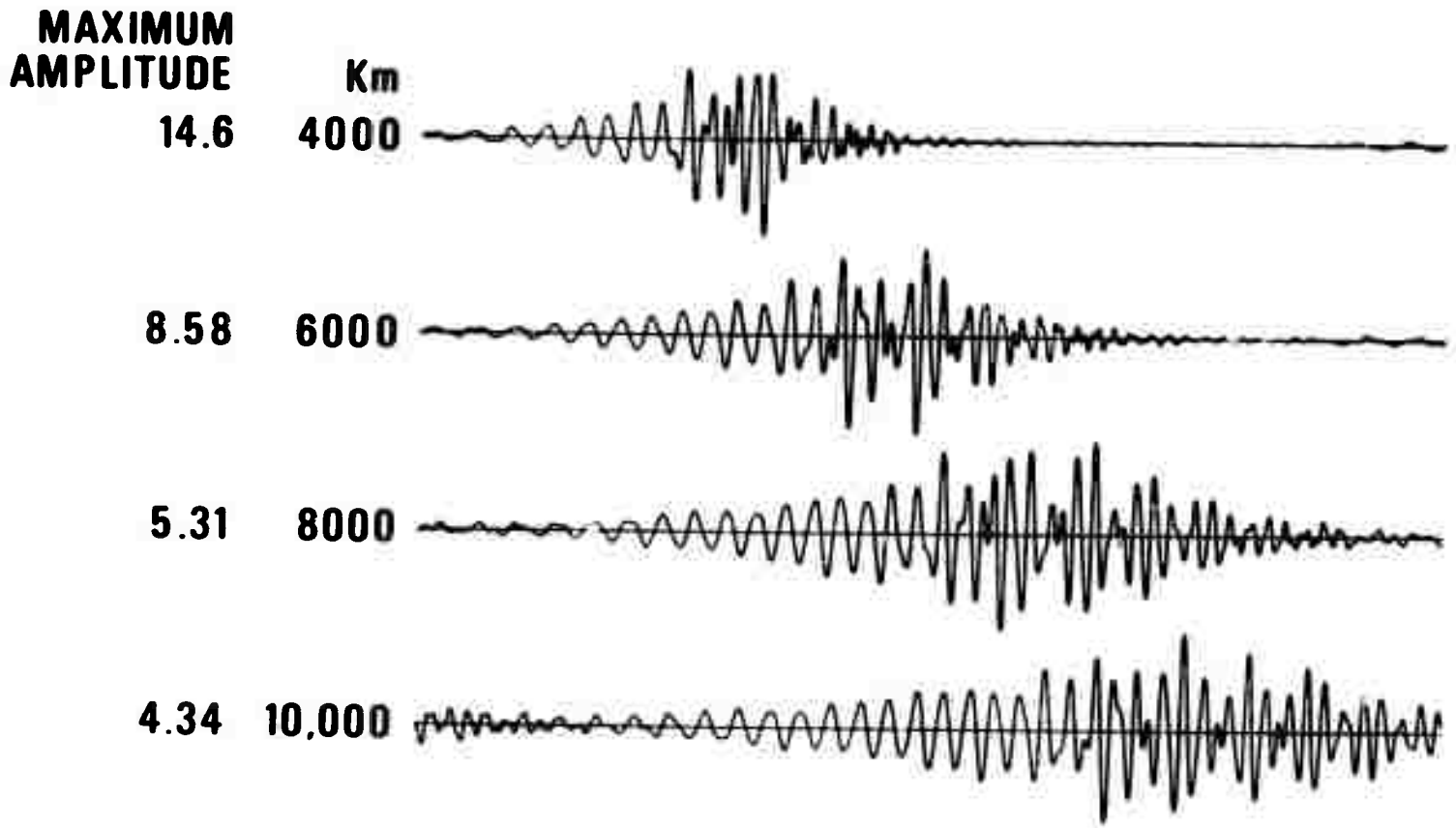

Figure 5c (cont'd.) Synthetic fundamental-mode Rayleigh-wave signals for a high-Q mid-continental structure at various epicentral distances.

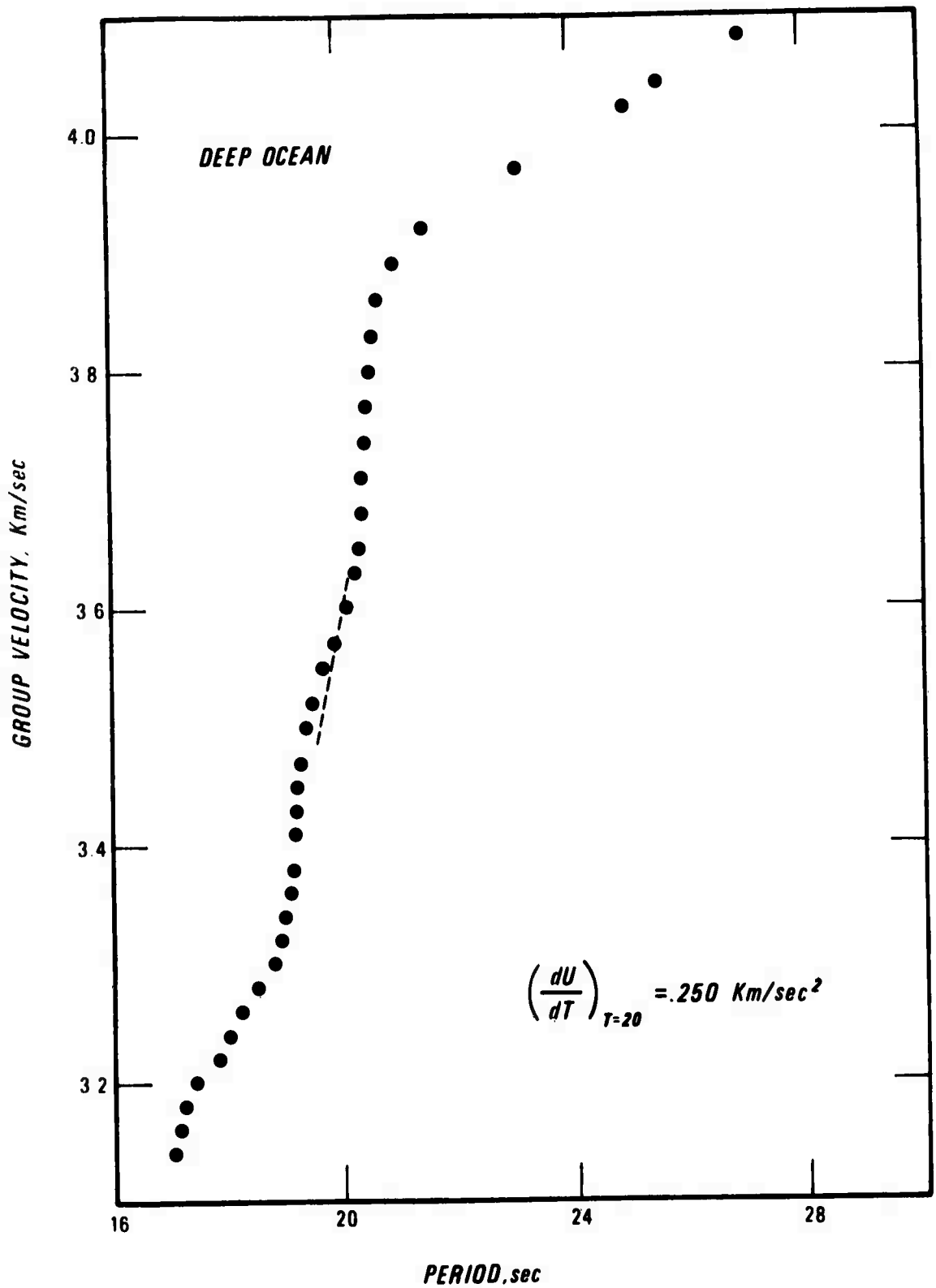

Figure 6. Group velocity versus period as measured on the 10,000 km synthetic seismograms of Figures 5a and 5b.

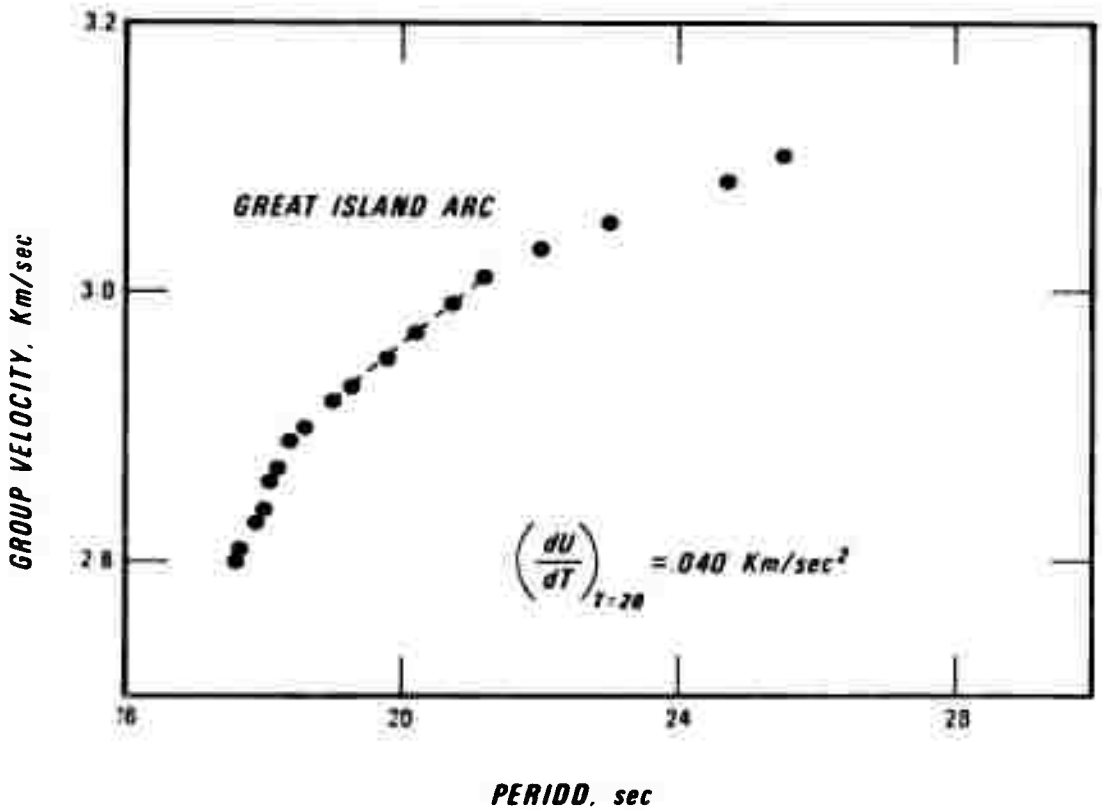

Figure 6 (cont'd.). Group velocity versus period as measured on the 10,000 km synthetic seismograms of Figures 5a and 5b.

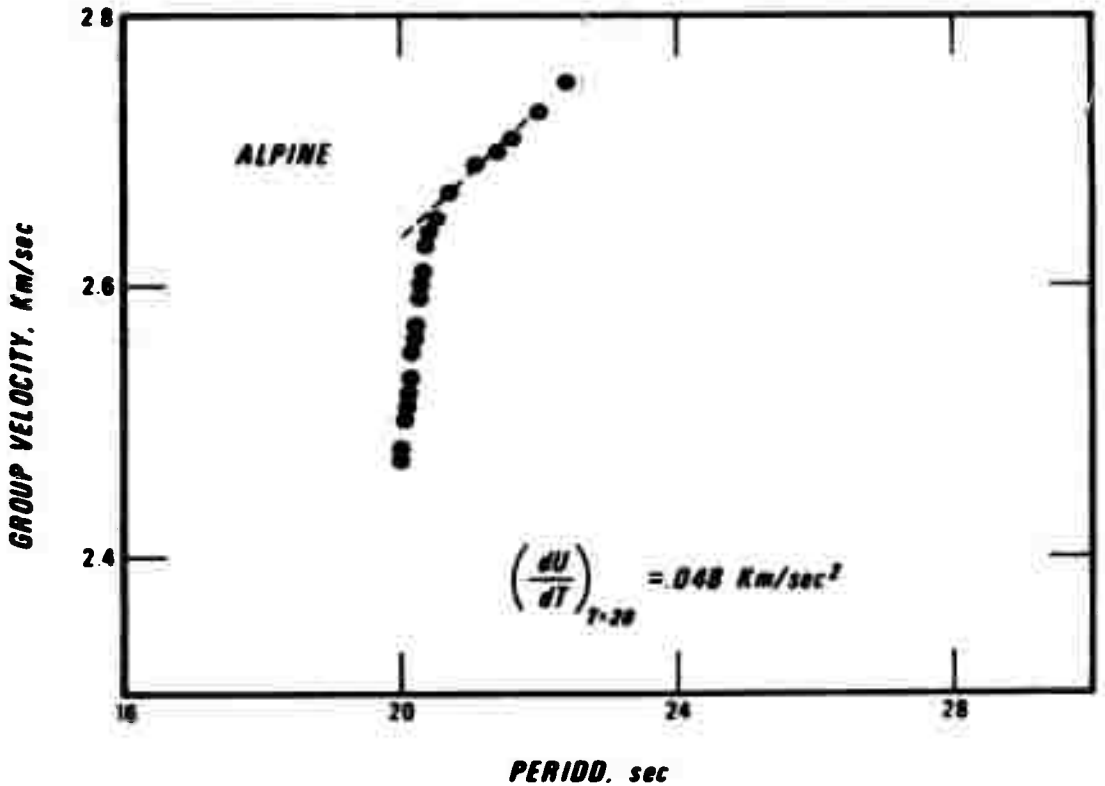

Figure 6 (cont'd.). Group velocity versus period as measured on the 10,000 km synthetic seismograms of Figures 5a and 5b.

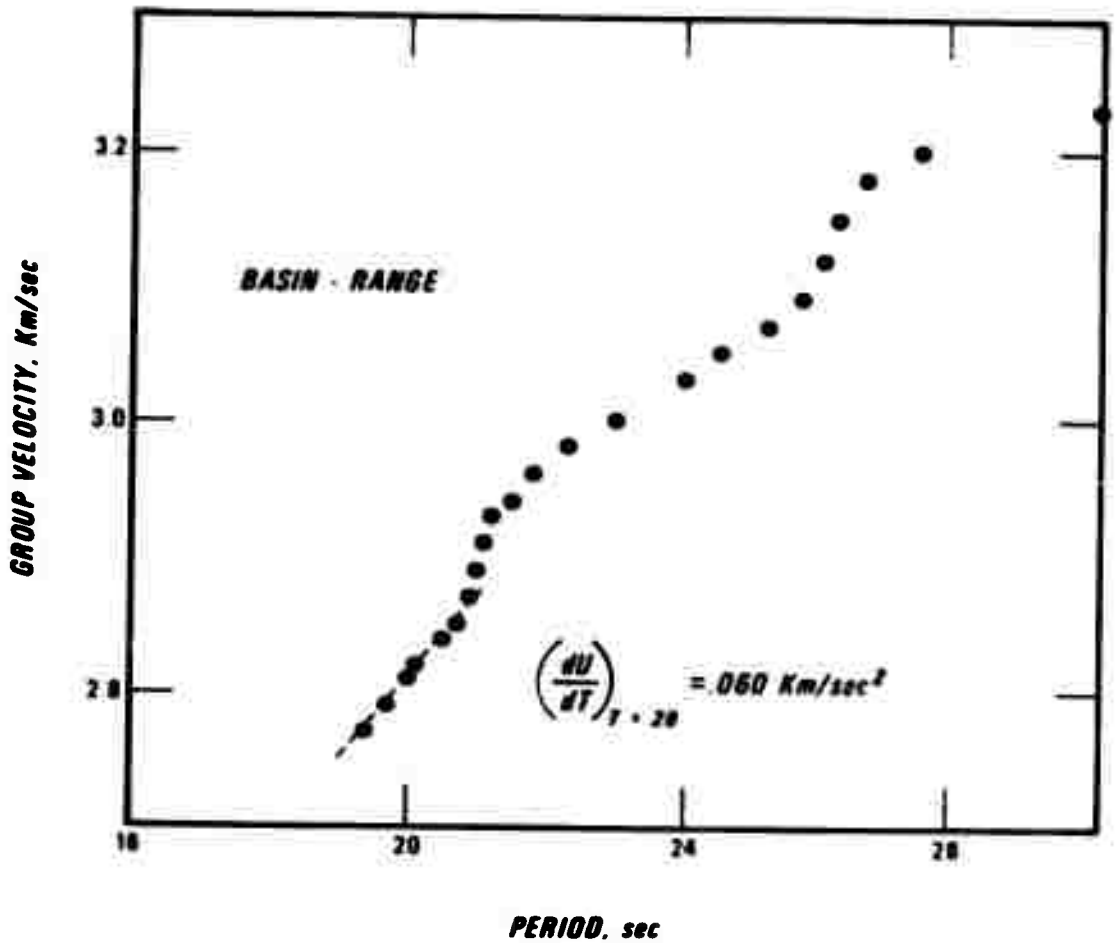

Figure 6 (cont'd.). Group velocity versus period as measured on the 10,000 km synthetic seismograms of Figures 5a and 5b.

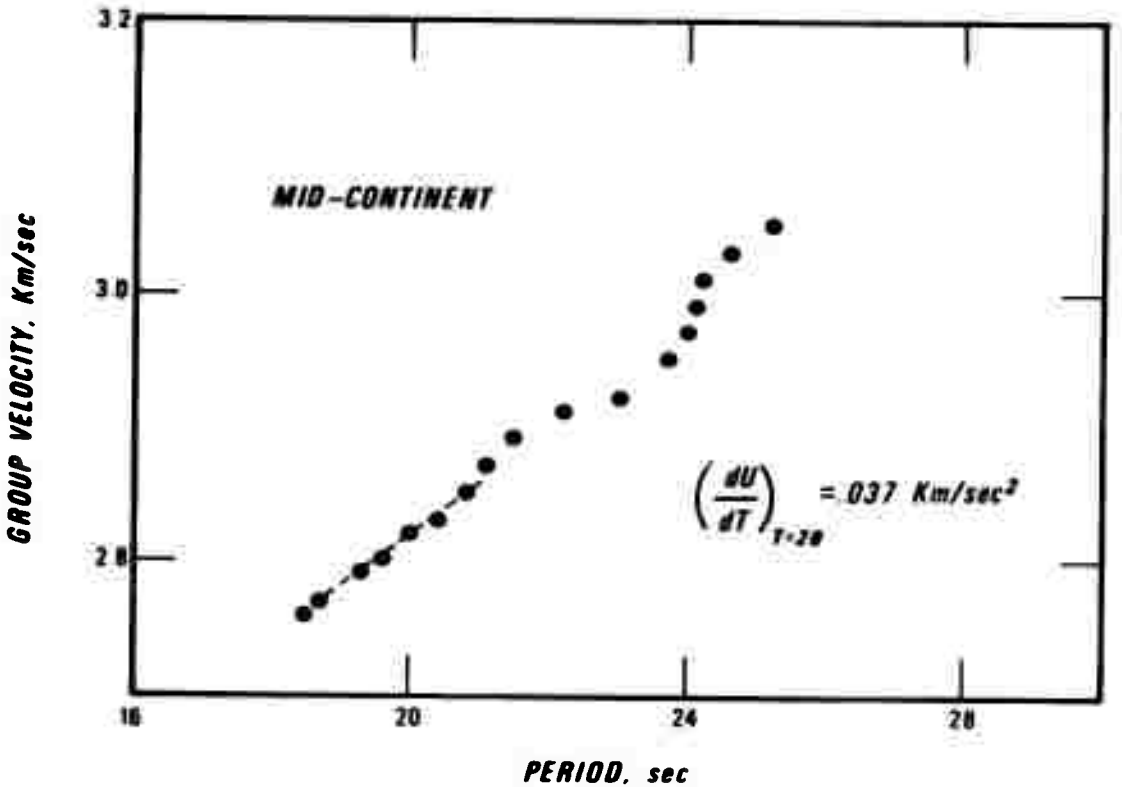

Figure 6 (cont'd.). Group velocity versus period as measured on the 10,000 km synthetic seismograms of Figures 5a and 5b.

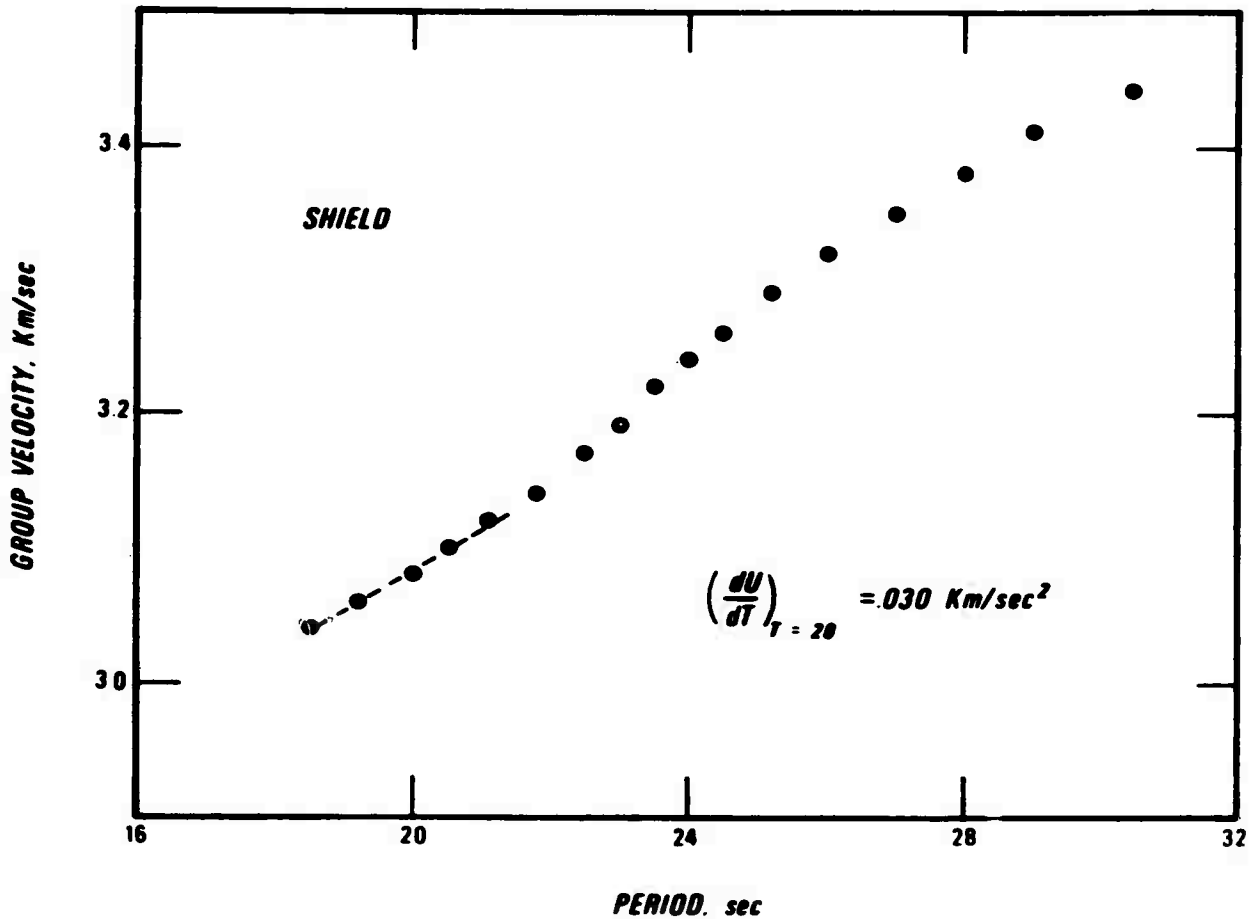

Figure 6 (cont'd.). Group velocity versus period as measured on the 10,000 km synthetic seismograms of Figures 5a and 5b.

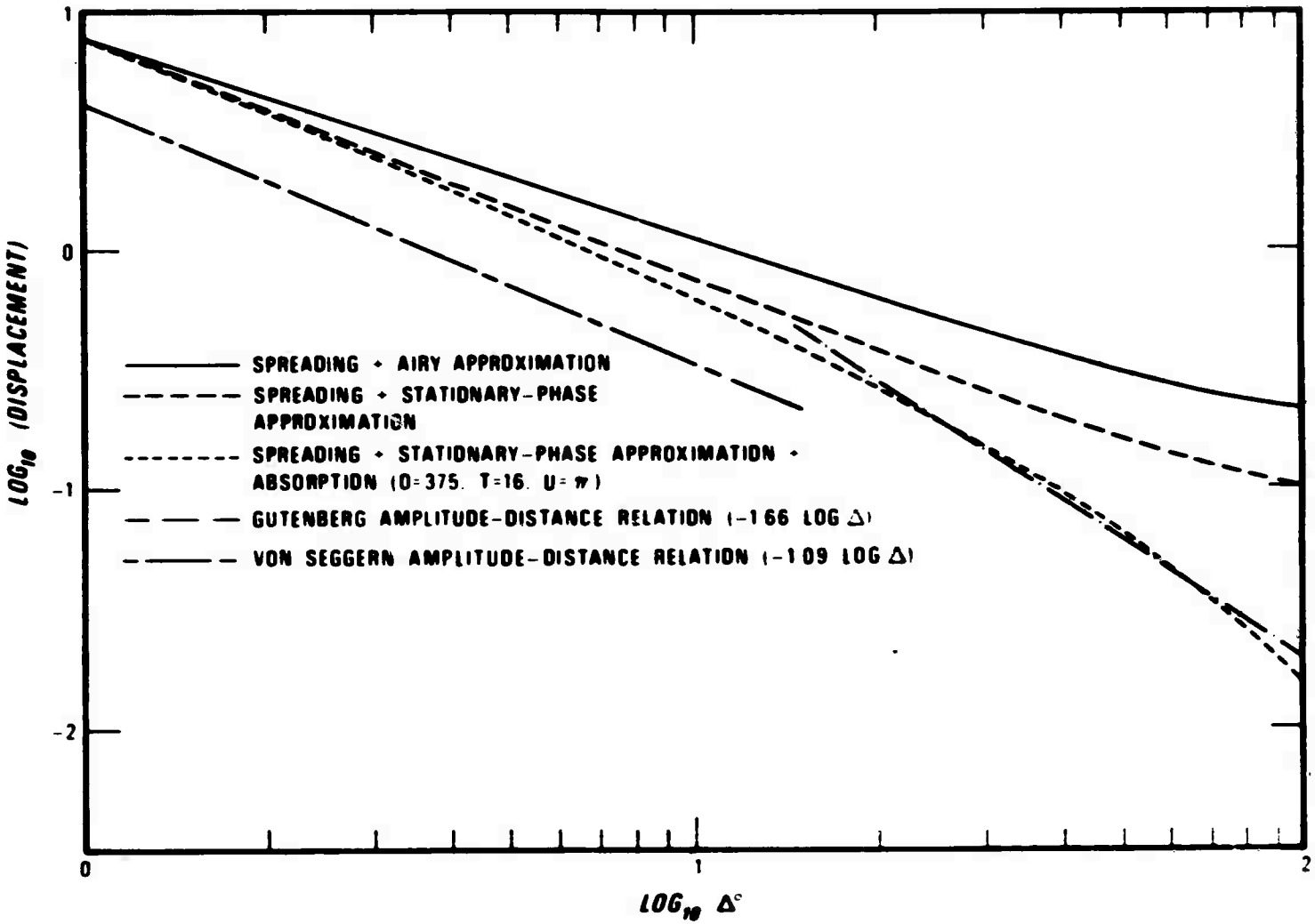

Figure 7. Theoretical amplitude-distance relations for maximum amplitudes of Rayleigh-wave signals compared to Gutenberg's (1945) and von Seggern's (1970) empirical relations.

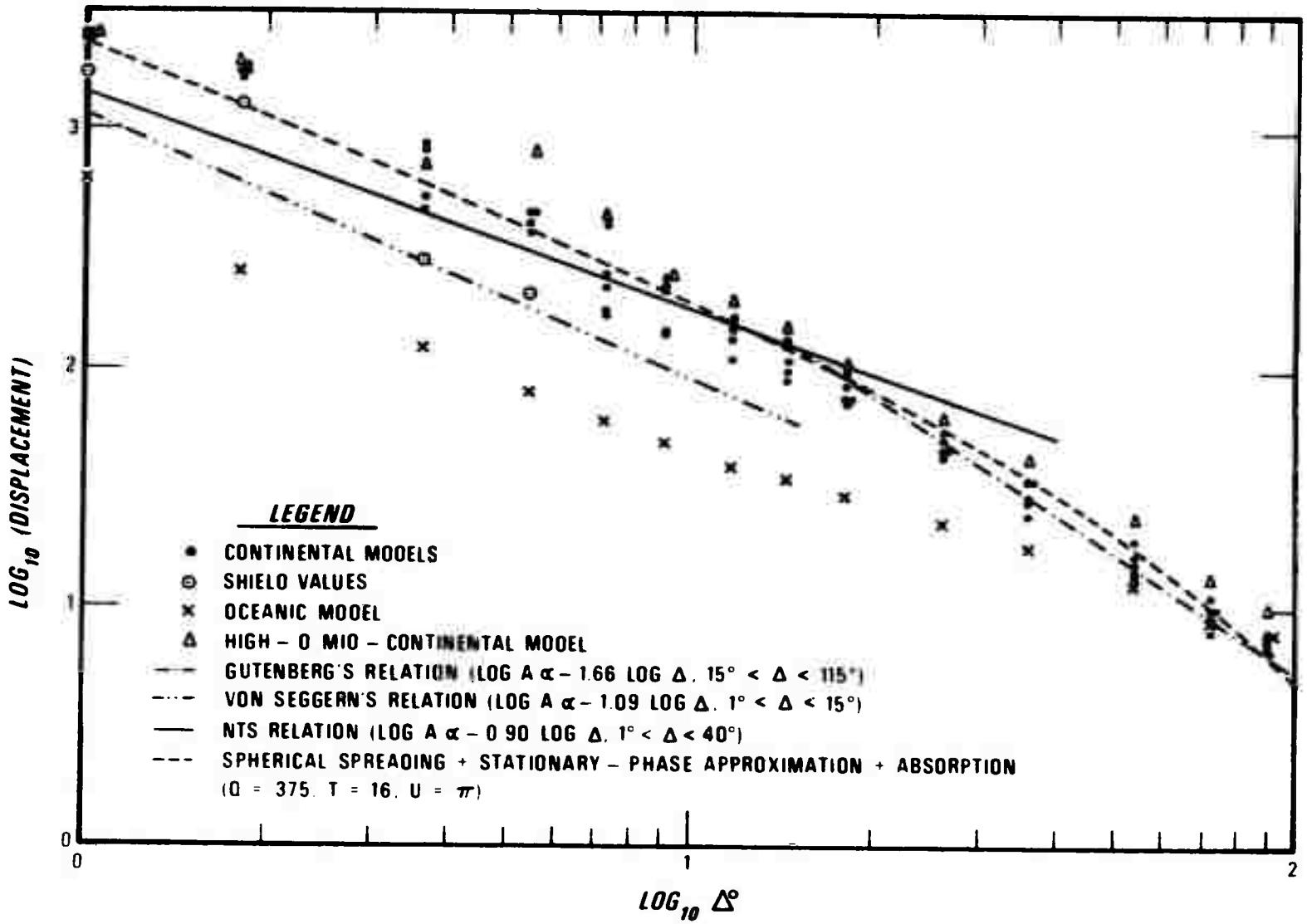

Figure 8. Measured maximum amplitudes from the synthetic seismograms of Figures 5a, 5b and 5c compared to theoretical and empirical amplitude-distance relations.

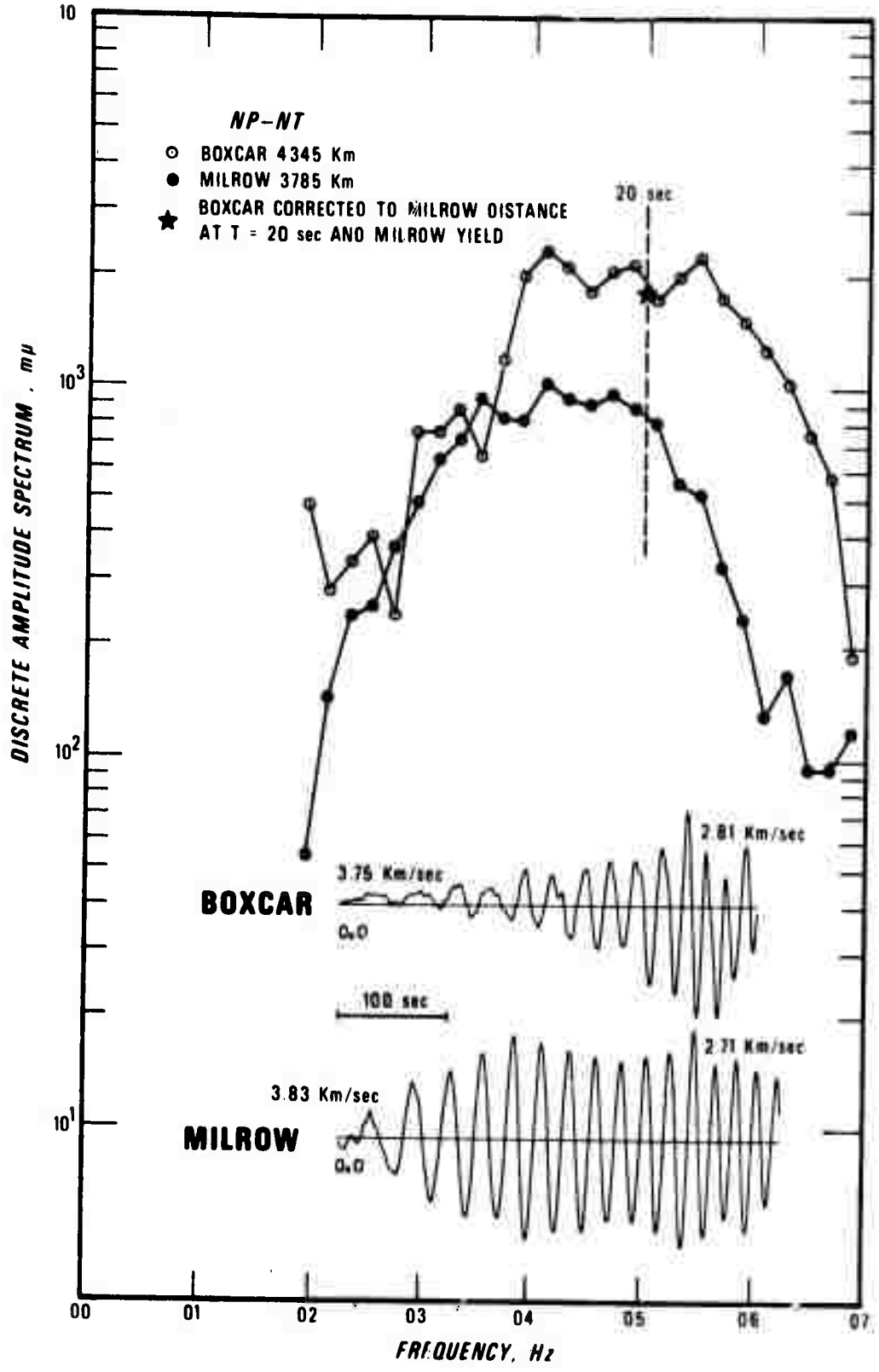

Figure 9. Spectra of BOXCAR and MILROW Rayleigh waves at NP-NT, WH2YK, PG2BC, RK-ON, and HN-ME.

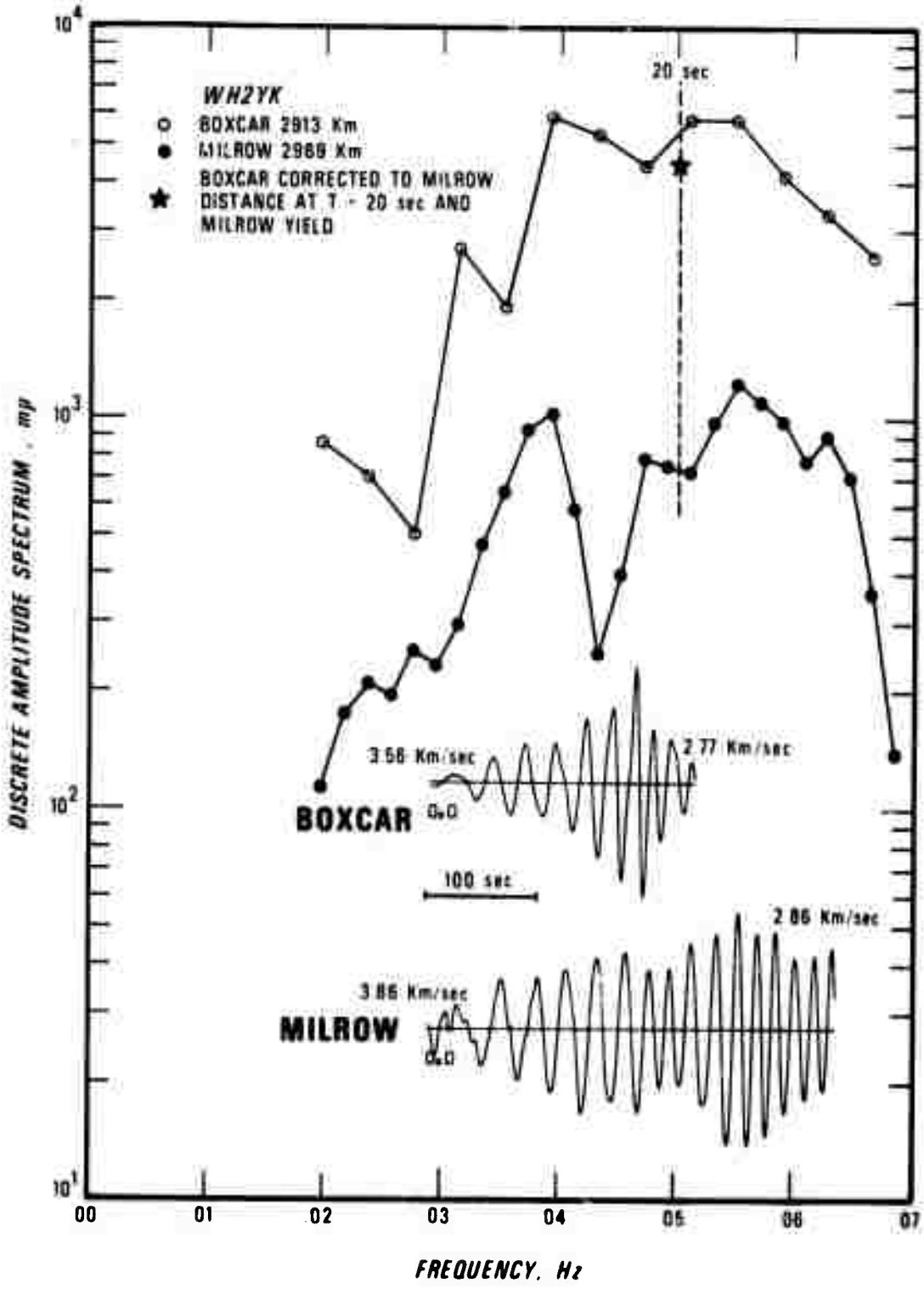

Figure 9 (cont'd.). Spectra of BOXCAR and MILROW Rayleigh waves at NP-NT, WH2YK, PG2BC, RK-ON, and HN-ME.

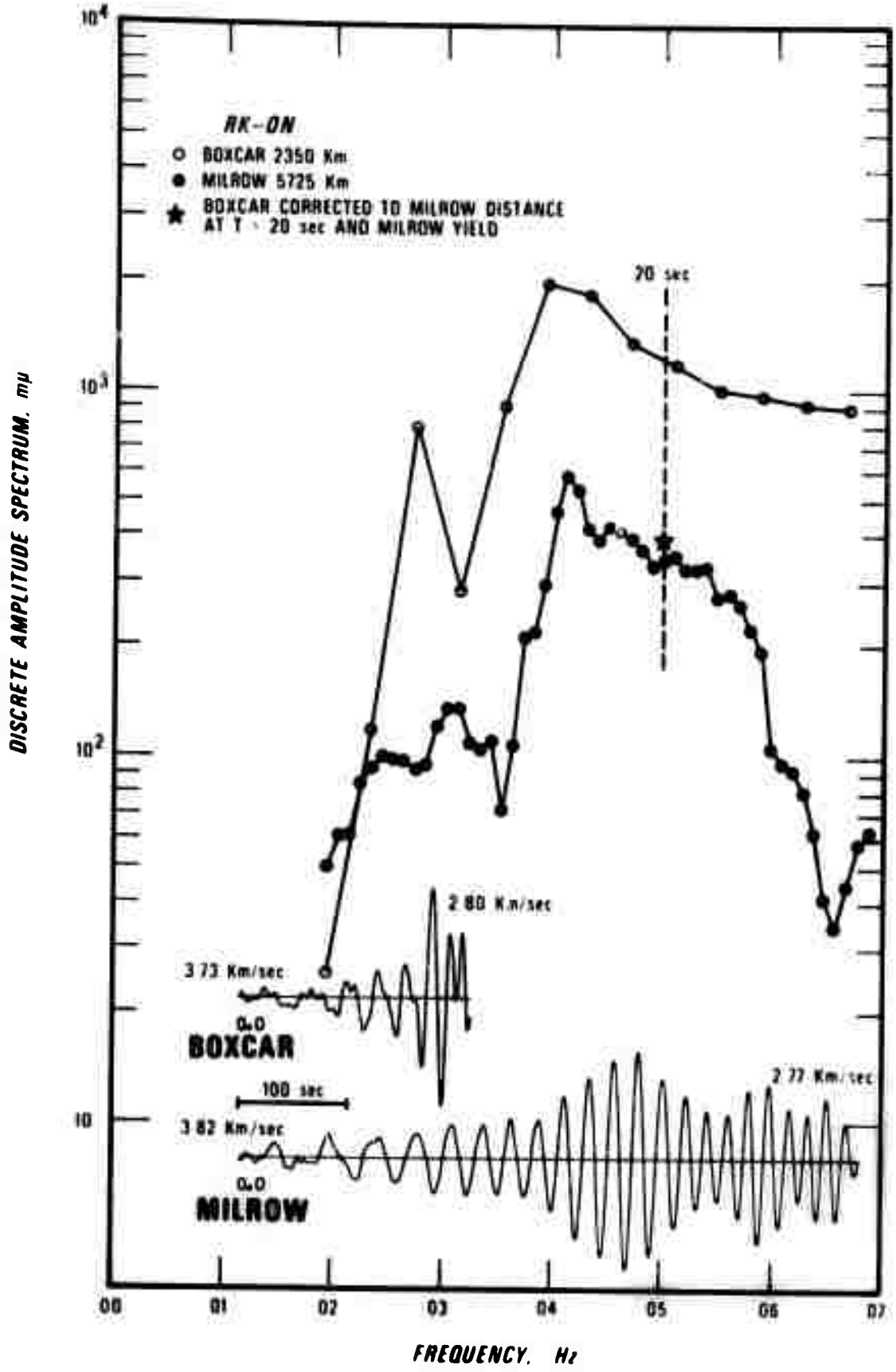

Figure 9 (cont'd.). Spectra of BOXCAR and MILROW Rayleigh waves at NP-NT, WH2YK, PG2BC, RK-ON, and HN-ME.

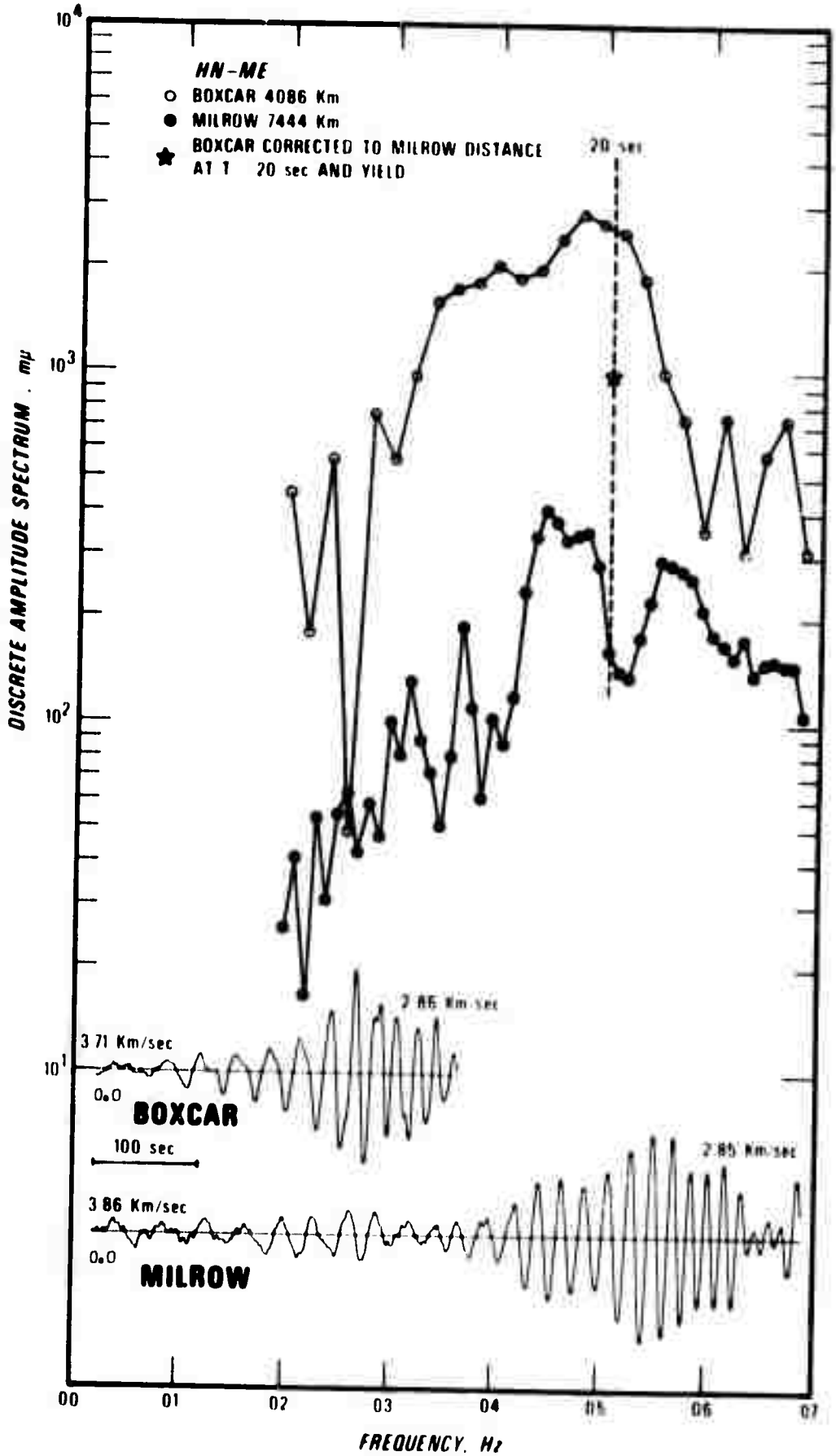

Figure 9 (cont'd.). Spectra of BOXCAR and MILROW Rayleigh waves at NP-NT, WH2YK, PG2BC, RK-ON, and HN-ME.

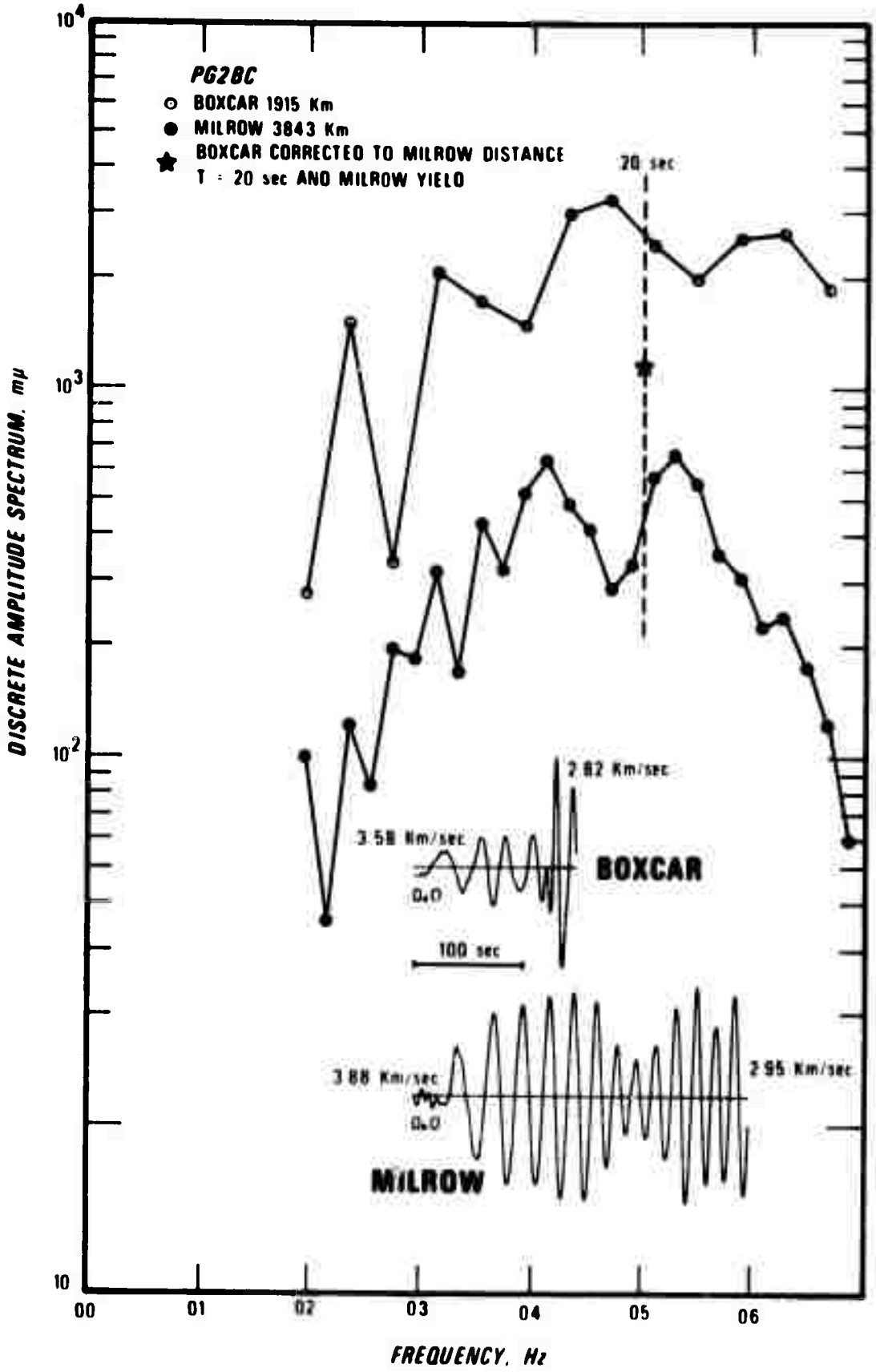

Figure 9 (cont'd.). Spectra of BOXCAR and MILROW Rayleigh waves at NP-NT, WH2YK, PG2BC, RK-ON, and HN-ME.

APPENDIX

DERIVATION OF STATIONARY-PHASE APPROXIMATION

Equation (6) in the text gave the expression for the fundamental-mode Rayleigh-wave signal from an explosion. Let $d\omega = Udk$ and $\omega/C = k$ in that expression to obtain:

$$w(r,t) = \frac{a^3}{R_o^{1/2} \sin^{1/2}(r/R_o)} \int \frac{P\varepsilon_o A_R G U \omega^{1/2} \exp[i(\omega t - kr) - \phi - 5\pi/4]}{C^{1/2} \exp[-\omega r/2Q(\omega)U(\omega)]} dk \tag{A1}$$

This can be compared with a similar expression in Båth (1969, p. 44, equation (9)). We must now assume that all the factors in the integrand except the eikonal function vary slowly with wavenumber $\underline{k}$. The stationary-phase approximation for (A1) is then given by reference to Båth again (p. 45, equation (13)):

$$w(k,r) = \frac{a^3 P\varepsilon_o A_R G U \omega^{1/2} \cos(\omega t - kr - \phi - 5\pi/4 \pm \pi/4)}{C^{1/2} R_o^{1/2} \sin^{1/2}(r/R_o) \exp(-\omega r/2QU) \left| \frac{\pi r \, d^2\omega}{2U \, dk^2} \right|^{1/2}} \tag{A2}$$

where we have replaced t by r/U in Båth's expression. The positive sign applies to normal branches of the dispersion curve, the negative sign to inverse branches. We desire to express ω in terms of period T_o rather than wavenumber k_o. Since $U = d\omega/dk$, we can write:

$$\frac{d^2\omega}{dk^2} = \frac{dU}{dk}$$

or

$$\frac{d^2\omega}{dk^2} = U \frac{dU}{d\omega} \qquad \text{(A3)}$$

From the definition $\omega = 2\pi/T$

$$d\omega = - \frac{2\pi dT}{T^2}$$

Thus (A3) becomes

$$\frac{d^2\omega}{dk^2} = - \frac{UT^2}{2\pi} \frac{dU}{dT} \qquad \text{(A4)}$$

Substituting (A4) in (A2) and using $k = 2\pi/CT$ and $\omega t = 2\pi r/UT$:

$$w(T,r) = \frac{a^3 P \varepsilon_o A_R G U \omega^{1/2} \cos(2\pi r/UT - 2\pi r/CT - \phi - 5\pi/4 \pm \pi/4)}{C^{1/2} R_o^{1/2} \sin^{1/2}(r/R_o) \exp(-\pi r/QUT) \left| \frac{rT^2}{4} \frac{dU}{dT} \right|^{1/2}}$$

Simplifying, we have

$$w(T_1,r) = \frac{\pi^{1/2} a^3 P \varepsilon_o A_R G U \cos[(2\pi r/T)(1/U - 1/C) - \phi - 5\pi/4 \pm \pi/4]}{2^{1/2} C^{1/2} R_o^{1/2} \sin^{1/2}(r/R_o) \exp(-\pi r/QUT) \; T^{3/2} \left| \frac{dU}{dT} \right|^{1/2}}$$

The form of equation (8) in the text follows if we assume that all the factors are constant except those determining the dispersion, namely, U and C.